Quantitative magnetic resonance (MR) neurography for evaluation of peripheral nerves and plexus injuries

Teodoro Martín Noguerol[1], Rafael Barousse[2], Mariano Socolovsky[3], Antonio Luna[1,4]

[1]MRI Unit, Neuroradiology Section, Clínica Las Nieves, SERCOSA, Health Time, Jaén, Spain; [2]Peripheral Nerve and Plexus Department, Centro Rossi, Buenos Aires, Argentina; [3]Peripheral Nerve and Plexus Surgery Unit, Department of Neurosurgery, University of Buenos Aires School of Medicine, Buenos Aires, Argentina; [4]Department of Radiology, University Hospitals of Cleveland, Case Western Reserve University, Cleveland, OH, USA

Correspondence to: Teodoro Martín Noguerol. MRI Unit, Neuroradiology Section, Clínica Las Nieves, SERCOSA, Health Time, Calle Carmelo Torres, 2 C.P. 23007, Jaén, Spain. Email: t.martin.f@htime.org.

Abstract: Traumatic conditions of peripheral nerves and plexus have been classically evaluated by morphological imaging techniques and electrophysiological tests. New magnetic resonance imaging (MRI) studies based on 3D fat-suppressed techniques are providing high accuracy for peripheral nerve injury evaluation from a qualitative point of view. However, these techniques do not provide quantitative information. Diffusion weighted imaging (DWI) and diffusion tensor imaging (DTI) are functional MRI techniques that are able to evaluate and quantify the movement of water molecules within different biological structures. These techniques have been successfully applied in other anatomical areas, especially in the assessment of central nervous system, and now are being imported, with promising results for peripheral nerve and plexus evaluation. DWI and DTI allow performing a qualitative and quantitative peripheral nerve analysis, providing valuable pathophysiological information about functional integrity of these structures. In the field of trauma and peripheral nerve or plexus injury, several derived parameters from DWI and DTI studies such as apparent diffusion coefficient (ADC) or fractional anisotropy (FA) among others, can be used as potential biomarkers of neural damage providing information about fiber organization, axonal flow or myelin integrity. A proper knowledge of physical basis of these techniques and their limitations is important for an optimal interpretation of the imaging findings and derived data. In this paper, a comprehensive review of the potential applications of DWI and DTI neurographic studies is performed with a focus on traumatic conditions, including main nerve entrapment syndromes in both peripheral nerves and brachial or lumbar plexus.

Keywords: Magnetic resonance imaging (MRI); diffusion MRI; diffusion tensor imaging (DTI); peripheral nerve; plexus

Introduction

Peripheral nerves (PN) and plexus injuries are commonly involved in patients with major, or even, minor trauma. The overall prevalence of PN injury in patient which suffer multiple trauma can reach up to the 5% (1). These lesions usually affect upper limbs, especially brachial plexus, but also ulnar or median nerves, being less common the lesion of lower limbs nerves or lumbar plexus. Clinical and electrophysiological exams are usually the first diagnostic step in the evaluation of PN or plexus injuries. However, due to the complexity of the injury mechanism and the delay in the setting of the symptoms and electrophysiological changes, it is not easy to establish an accurate diagnosis of the exact injury site and PN damage

severity. At this point, morphological imaging techniques, such as ultrasonography (US) and magnetic resonance imaging (MRI), allow an adequate visualization of PN and its pathologic conditions (2). US has the main advantage of its accessibility with appropriate spatial and temporal resolution, but is highly dependent on the operator skills and experience. Moreover, US only allows evaluating with confidence, superficial PN or brachial plexus in its proximal segments and in patients with major injuries and open wounds PN, these structures are not always identified by US as desired. Morphological MRI neurography, based on high-resolution 3D sequences with or without fat suppression techniques, has the potential to provide important information for PN assessment. However, morphological sequences have shown limitations for PN lesion detection or characterization in certain scenarios, such as apparent healthy PN with altered function or otherwise, areas of increase of signal intensity within PN on fat suppression studies influenced by magic angle effect, without real clinical relevance (3). In the era of functional imaging, new MRI sequences have allowed adding further information beyond the conventional morphological evaluation, not only of the central nervous system (CNS) (4), but also of PN. Recent neurographic techniques based on diffusion weighted imaging (DWI) and diffusion tensor imaging (DTI) have supposed a qualitative and quantitative leap for PN and plexus evaluation using functional neurography.

For traumatic conditions, such as PN extrinsic compression or postsurgical status, functional neurography can help to identify the specific area of PN injury, and also to assess the underlying pathophysiology of the injured nerves. The morphological and functional data derived from DWI or DTI reflect a wide spectrum of pathophysiological conditions and properties within the PN, such as myelin integrity, axonal conduction, edema or nerve structure integrity, that may be quantified for different clinical applications (5,6). Thus, this information may define in a more accurate way, crucial questions for the clinician dealing with PN injury: (I) the possible etiology of PN damage; (II) rule out other potential causes of PN injuries and (III) predict or monitor the patient outcome in the case of conservative or surgical treatment.

In this review, the physical basis of DWI and DTI for functional neurography acquisition is discussed. Moreover, the application of these techniques in several clinical scenarios is also analyzed, emphasizing on the derived quantitative parameters, how to calculate them and their biological meaning for PN and plexus injury evaluation.

Technical considerations

DWI neurography

PN are highly anisotropic structures with a marked diffusion restriction in its perpendicular plane and facilitated diffusion along its main axis (7). These physiological features allow to use DWI for the study of PN, lumbar or brachial plexus. DW-based neurography (DWN) benefits from the use of gradients with the maximum strength to maintain the high signal of PN, while reducing the signal of surrounding tissues (8). PN and plexus can be highlighted from the rest of adjacent structures by applying one or two motion probe gradients perpendicular to the course of the nerve (*Figure 1*). In DWN, a high b value between 500 to 1,000 s/mm^2, usually b 800 s/mm^2, is acquired providing a good signal to noise ratio (SNR) and adequate suppression of neighboring structures (9). The inclusion of a fat-suppression technique in DWN sequences is mandatory, which may be performed using spectral or non-spectral fat suppression techniques. Diffusion weighted imaging with background signal suppression (DWIBS), a sequence designed particularly for whole-body applications, benefits from the use of short-tau inversion recovery (STIR), a non-selective, non-spectral fat suppression technique to increase the contrast of nerve structures with background structures, allowing at the same time to studying wider fields of view than DWN sequences based on spectral fat suppression techniques such as spectral presaturation with inversion recovery (SPIR) or spectral attenuated inversion recovery (SPAIR), which can be used for specific evaluation of determined anatomical regions (10).

DWN provides quantitative data by means of the apparent diffusion coefficient (ADC). For this aim, it is necessary to include in the acquisition a low b value, usually ranging between 0 to 50 s/mm^2. ADC may help to confirm and quantify the presence of edema in PN trauma or compression (11) and characterize tumoral lesions (12).

DWN allows an accurate anatomical representation of PN by means of a fast and easy post process. Using an algorithm with maximum intensity projection (MIP) reconstruction of the obtained dataset, the PN are nicely shown, employing either conventional grey scale, or in the case of brachial or lumbar plexus inverted grey scale can be used for a better display.
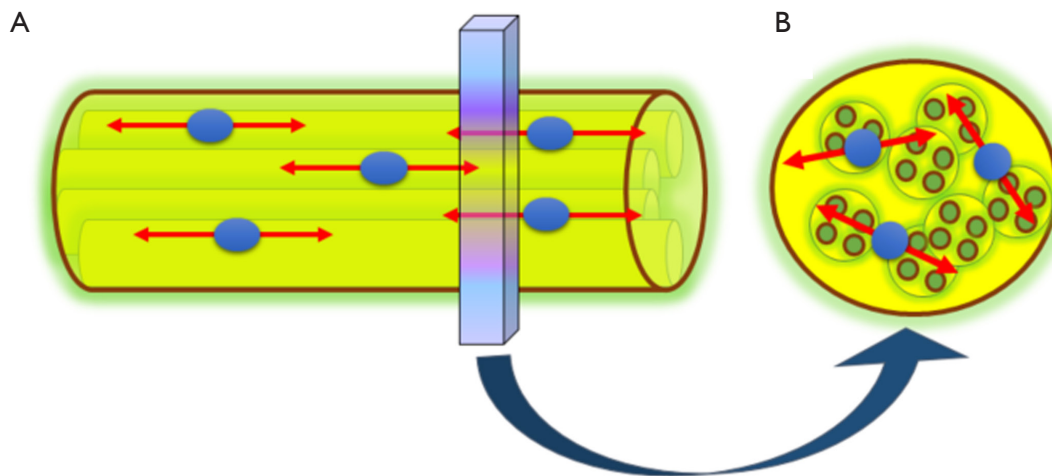
Figure 1 Water diffusion within PN scheme. (A) Water diffusivity is facilitated along the main (longitudinal) axis of PN; (B) if motion probe gradients are applied perpendicular to the course of these PN, DWI will show restriction of water molecule movement in the short axis due to the presence of physiological barriers such as myelin sheaths. PN, peripheral nerves; DWI, diffusion weighted imaging.

DTI neurography

A different approach for the study and representation of PN is the use of DTI, a technique that has been widely used for the assessment of CNS, and in recent years, also in spinal cord (13-15). As discussed above, PN are highly anisotropic structures, presenting a facilitated diffusion along its longitudinal axis and a marked restriction of the free movement of water in the transverse plane. In order to characterize and quantify the water movement within nerves, it is necessary to acquire at least six diffusion directions with a maximum b value ranging from 800 to 1,200 s/mm^2. The dominant direction is given by the principal eigenvector, and the other two perpendicular directions by two secondary eigenvectors (16). With these eigenvectors, which are the directional expression of a certain eigenvalues, several parameters can be calculated (*Figure 2*). Fractional anisotropy (FA) is the commonest used by radiologists. Other derived parameters from DTI are mean diffusivity (MD), axial diffusivity (AD) and radial diffusivity (RD), each one of those reflects a different property of the PN as it will be described below, and can be used as biomarkers of PN damage or regeneration (17).

The evaluation of the fibers compounds of PN with DTI-neurography (DTN) is useful in the study of traumatic or tumor conditions. 3D neurographic reconstructions can be performed from DTI data, in a similar fashion to tractography of the CNS, helping for PN structure evaluation and assessment of its relationship with other neighboring structures.

DWN vs. DTN

DTN can be considered as an upgraded evolution of DWN. DWN provides mainly information about axonal fibers integrity from a qualitative point of view. However, DWN and ADC, its main derived parameter, offer scarce information regarding the movement direction of water within the axon. The acquisition of multiple diffusion directions in DTN provides more complex parameters, such as FA or MD, that allow a more precise understanding of the pathophysiology of water diffusion and axonal flow direction. In addition, 3D neurographic reconstructions suppose an added value that gives novel information of PN microstructure that can be used to evaluate their relationship with normal or abnormal neighboring structures, the presence of neurogenic tumors or traumatic lesions (18).

DWN can be integrated in conventional protocols, especially for brachial and lumbar plexus evaluation, thanks to its faster acquisition, larger coverage area and easier post process in comparison to DTN. DTN provides multidirectional information and more robust data for quantification. In clinical practice, DTN should be used when a precise anatomical detail of nerve structure or more accurate quantification is needed. *Table 1* resumes the main advantages and disadvantages for using DWN and DTN.
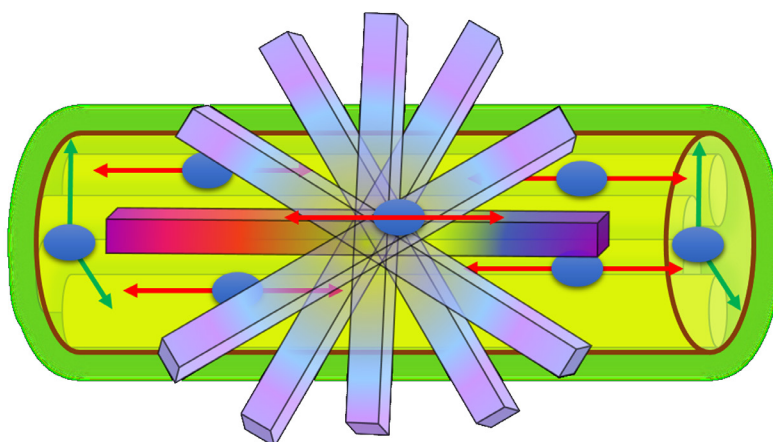
Figure 2 DTI for PN evaluation. The use of motion probing gradients in multiple (at least 6) directions allows assessing the main direction of water diffusion that correlates with the main eigenvector (red arrows), as well as the other two perpendicular minor eigenvectors (green arrows). DTI, diffusion tensor imaging; PN, peripheral nerves.

Table 1 Advantages and disadvantages of functional neurographic sequences

Neurographic sequence	Advantages	Disadvantages
DWI neurography	High background signal contrast ratio	Low spatial resolution
	Allows large field of view with short acquisition times	Contamination with other hyperintense structures on DWI
	Easy post process	T2 shine-through effect
	Quantification: ADC	Low specificity of ADC
DTI neurography	High anatomical detail	Prone to artifacts
	Quantification: FA, MD, AD and RD which increase sensitivity and specificity	Small field of view with long acquisition times
		Time consuming post process

DWI, diffusion weighted imaging; ADC, apparent diffusion coefficient; DTI, diffusion tensor imaging; FA, fractional anisotropy; MD, mean diffusivity; AD, axial diffusivity; RD, radial diffusivity.

Biological meaning of derived parameters

Several parameters are derived from DWN and DTN studies, which allow quantifying diverse pathophysiological conditions in PN (*Figure 3*).

ADC

ADC results from the difference in signal intensity terms between both the low and the high b values. ADC reflects the water displacement in the extracellular space without consideration of water molecules motion direction (19). High ADC values are consistent with increase of this extracellular space, usually representing edema regardless of its origin (i.e., trauma, compression or fiber disruption). ADC is expressed in mm^2/s, and allows quantifying and monitoring the edema within PN or plexus. In PN pathology, it is less common to find low ADC values, which usually indicates the presence of a solid lesion with reduced extracellular space such as neurogenic tumors (20).

FA

FA is an index of fiber organization, which reflects the integrity of axonal bundles and the directionality of water movement delimited by physiological barriers such as myelin sheaths, endoneurium, perineurium or epineurium. FA is a dimensionless parameter, which values vary from
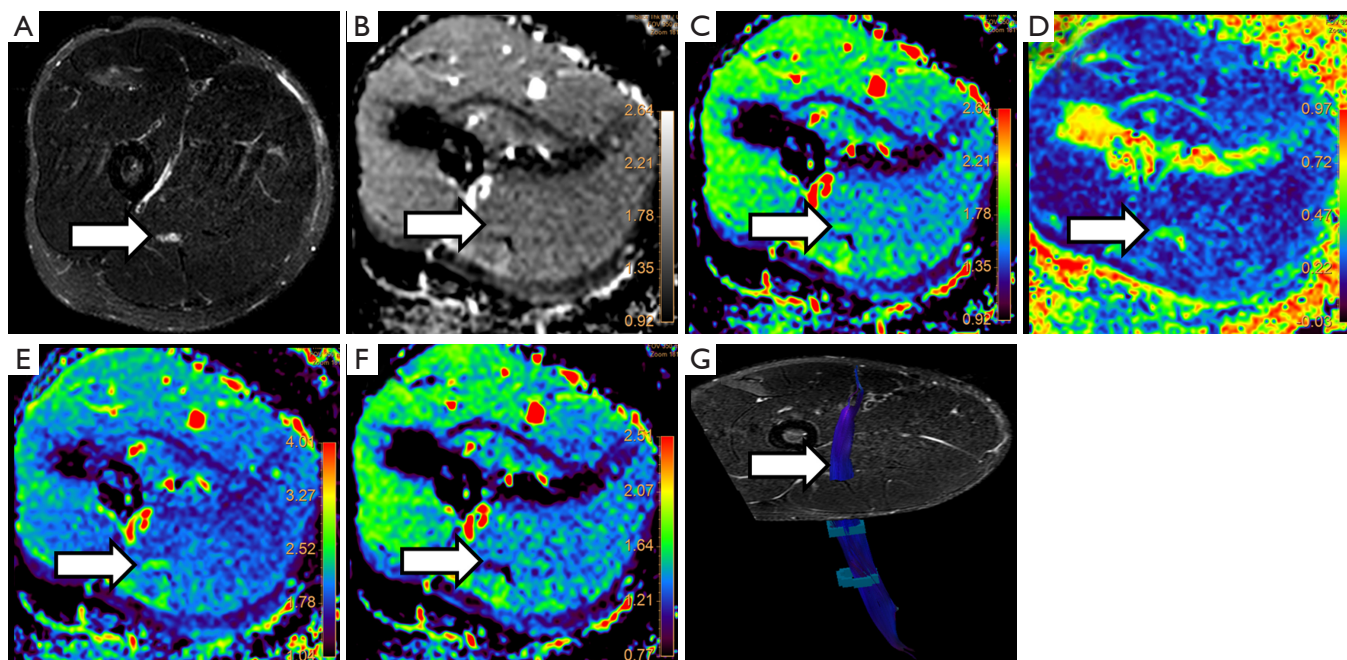
Figure 3 DWI and DTI derived parametric maps and values in a healthy sciatic nerve (arrows). (A) Axial STIR of proximal right thigh shows normal sciatic nerve (white arrow); (B) ADC and (C) MD maps show values of 2.20×10^{-3} and 2.10×10^{-3} mm²/s, respectively; (D) FA demonstrates a value of 0.6 within normal limits for a healthy PN; (E) AD value corresponds to 3.01×10^{-3} mm²/s as water diffusivity is facilitated along the main axis of sciatic nerve; (F) however, RD shows a value of 1.03×10^{-3} mm²/s due to the restriction of water diffusion within the perpendicular axis; (G) DTI also permits to perform a 3D neurographic reconstruction using a ROI based model, which shows a well delimited fibrillar structure at the posterior aspect of the thigh, coded with blue color by consensus (head to toe main direction of water diffusion), consistent with sciatic nerve. STIR, short-tau inversion recovery; ADC, apparent diffusion coefficient; MD, mean diffusivity; FA, fractional anisotropy; PN, peripheral nerves; AD, axial diffusivity; RD, radial diffusivity; DTI, diffusion tensor imaging; ROI, region of interest.

0 to 1. An FA value of 0 is considered the lowest level of fiber organization, the highest isotropic diffusion. A FA value of 1 is related with the maximum anisotropy or the highest level of fiber organization (21). PN usually don't show the highest FA values because, as previously explained, there are other directions of water movement within the nerve fibers. However, healthy PN usually point FA values of about 0.6 with physiological variations depending on the evaluated (proximal or distal) area, the patient age and other factors. Previous reports have demonstrated that there is a variation in FA values that correlates with the age of the studied subjects (22). These variations have to be taken into account when DTI studies are used for PN evaluation in order to avoid false positive or negative results. FA has a very high sensitivity for lesion detection, even in apparent normal PN on conventional morphological studies (2).

MD

MD is a parameter derived from DTI that is the result of the average of the three main eigenvalues (23). As MD considers the main three directions of the space, allows assessing more accurately the water displacement at extracellular space in comparison to ADC, which does not consider any water direction. It is measured in the same units than ADC (mm²/s), with parallel behaviour of both parameters in different clinical scenarios.

AD

AD (mm²/s) corresponds to the measure of the main eigenvector. It reflects the water diffusion along the main nerve direction and can be consider a surrogate biomarker of axoplasmic flow integrity. In the main direction of PN, water can move freely as no barriers exists that impede its

motion, thus AD values are usually higher than ADC or MD ones (24). AD values may vary according to the type of PN injury and its location; in fact, theoretically, low AD values reflects a proximal interruption of axonal flow. However, it is not uncommon to find an increase of AD values secondary to the overall increase of water diffusion in neural damage (25,26).

RD

RD (mm^2/s) is the average of the two perpendicular (minor) eigenvalues. It reflects the degree of restriction or freedom of water diffusion within the short nerve axis. Due to the presence of myelin sheaths, the movement of water molecules in the perpendicular (short) axis is very limited (24). Thus, normal PN will show low RD values as they have it physiological barriers intact. In the other side, PN with traumatic or other kind of myelin damage will show higher RD values than normal PN as water molecules find no obstacles for free diffusion. In these terms, several studies have proposed to consider RD as a potential biomarker of myelin integrity not only for lesion detection but also for treatment monitoring. Normalization (decrease) of RD values in a damaged nerve may reflect a re-myelination process (27).

Clinical scenarios

The use of DWI based neurographic sequences has demonstrated several advantages over conventional morphological neurographic studies (9,18,28,29). The strength of these techniques relies on providing functional and quantitative information, allowing a correct understanding of the normal physiology of PN and the pathophysiological processes that underlie the different conditions involving PN, with potential influence to improve their diagnosis and therapy monitoring.

Peripheral nerve traumatic lesions

The diagnosis of traumatic injury of PN, including brachial and lumbar plexus is normally performed by a clinical examination followed by electrophysiological studies, mainly electroneurography. This latter type of exams is invasive, operator dependent and may show false negative results in the first phases after a PN injury. They are also limited to determine either the severity of a neural injury in the first 6 weeks following a nerve trauma (1), or the prognosis of that

lesion, which includes the differentiation between those that will recover spontaneously or those other which will require a surgical intervention. Signal intensity changes and patterns of denervation at muscular groups do not follow the same time course of nerve injuries and correlation between both findings is not always straightforward (30). Thus, morphological MRI is only able to show the presence of edema, and nerve thickening or disruption. DWN and DTN have also shown their ability to detect these morphological abnormalities in animal models, but adding pathophysiological and functional data (27). Further studies are needed to determine if these functional techniques may even detect abnormalities in PN without relevant findings on the conventional morphological studies as occurs in other anatomical areas such as in CNS or spinal cord (31,32).

PN can be injured by diverse external mechanisms such as compression, traction or transection (33), that may lead to different degrees of axonal lesion that in growing order of severity ranges from neuropraxia, axonotmesis to neurotmesis. The morphological classification of PN injuries performed by Seddon (34) and the histological adaptation carried out by Sunderland (35), are widely used for morphological evaluation of PN injuries and their pathophysiological changes are well described. For functional evaluation of PN using MRI, it is essential to correlate the pathophysiological changes that occur in each stage of PN injury with the parametric data derived from DWI and DTI studies. These data provide us valuable information about PN integrity or damage, nerve conduction capacity and involvement of myelin and collagen support structures such as perineurium, epineurium or endoneurium. DTN can also help to monitor PN damage as well to decide further therapeutic options (conservative treatment or surgery).

After PN trauma there is an increase of the water content at the extracellular space and a disruption of the collagen structure support. In this scenario, DWN may demonstrate thickening and focal increase of signal intensity of PN at higher *b* values compared with normal PN (*Figure 4*). ADC parametric maps demonstrate increase of ADC values reflecting the increase of water movement within the extracellular space at the site of nerve damage (36). In a similar manner, an increase of MD values will be found at the injured nerve segment. However, these parameters may appear insufficient for an adequate nerve evaluation and may not show statistically significant differences between each nerve segments. Thanks to the development of DTN sequences, diverse studies have demonstrated a
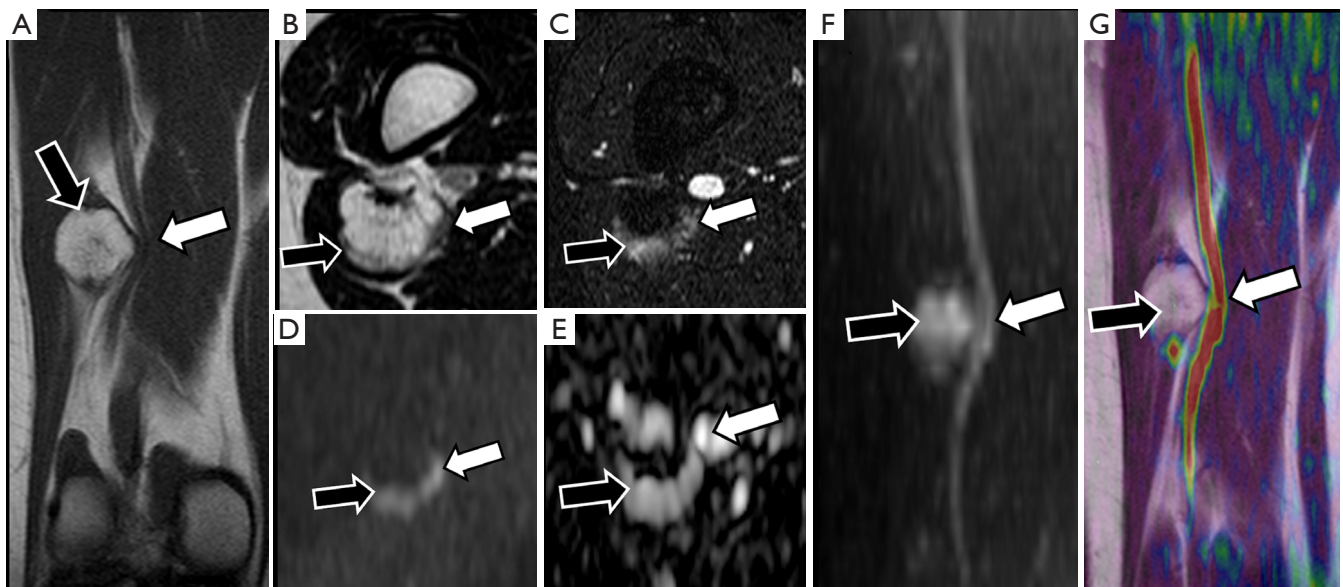
Figure 4 Sciatic nerve compression by femoral osteochondroma. A 26-year-old female with paresthesia at right lower limb underwent a MRI with DWN sequence. (A) Coronal TSE T1-weighted image shows a pedunculated lesion in the posterior aspect of the distal femur, which shows normal bone marrow content and a cartilage cap (black arrows) consistent with osteochondroma. This tumor contacts and displaces the sciatic nerve (white arrows); (B,C) axial TSE T2-weighted and STIR images confirm the compression of the sciatic nerve that shows moderate increase of its signal intensity (white arrows); (D,E) DWI with a *b* value of 800 s/mm^2 and corresponding ADC map demonstrate focal hyperintensity of sciatic nerve (white arrow), more evident at the site of compression by the osteochondroma, where an increase of ADC value (2.0×10^{-3} mm^2/s) is depicted consistent with edema; (F) coronal MPR of DWI with *b* value of 800 s/mm^2 allows obtaining a neurographic view of the sciatic nerve, demonstrating focal hyperintensity at the compression site (white arrow) and confirms its relation with the cartilaginous cap (black arrows); (G) fusion image of coronal T1-weighted sequence and DWI better shows all the described findings. MRI, magnetic resonance imaging; DWN, DW-based neurography; TSE, turbo-spin-echo; STIR, short-tau inversion recovery; DWI, diffusion weighted imaging; ADC, apparent diffusion coefficient; MPR, multiplanar reformation.

decrease of FA values, due to the loss of fiber anisotropy and the presence of edema (37). At the same nerve segment, an increase of RD is depicted due to the existence of a facilitated diffusion within the perpendicular plane owing to the disruption of physiological barriers that impeded the motion of water molecules in the short PN axis, mainly myelin sheaths but also endoneurium and perineurium (38) (*Figure 5*). This decrease of FA values and increase of RD values becomes more conspicuous at the compression site or traction/transection point, as well as in the distal segment, probably due to a Wallerian degeneration mechanism (39). These changes are less evident at proximal segments of the damaged nerve (37). Respecting AD, it might theoretically decrease at the distal segment of a damaged PN as there is interruption of the normal axonal flow (27). However, further studies are needed to confirm or reject this assumption (*Figure 6*).

In the continuum from neuropraxia to neurotmesis, a variation in FA and RD values may be found from subtle changes to more evident differences, finding lower FA values and higher RD values at more severe PN damage. This range of FA and RD values may help not only for the assessment of the severity of a PN injury, but also to suggest the time from trauma and also to sketch out the outcome of the nerve injury, even determining the choice between conservative or surgical treatment (38). Further experience with the use of this technique in a multidisciplinary team composed of neurosurgeons, neuro-electrophysiologists and radiologists is needed to establish cutoff points that can help in the decision between the different therapeutic options.

DTI has the added value to perform 3D reconstructions of PN. For PN injuries, 3D neurographic reconstructions may represent the structure of the damaged nerve. This representation may be useful for surgeons for treatment planning and assessment of the relationship of PN with
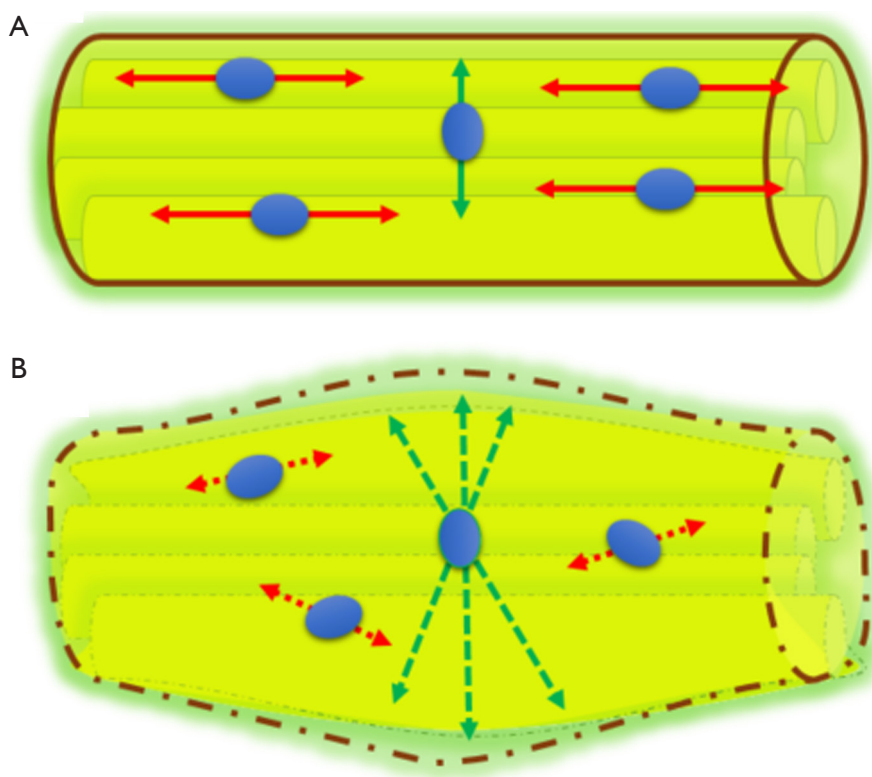
Figure 5 Pathophysiology of DTI findings in normal and injured PN. (A) Normal PN shows preserved axonal integrity with high FA values thanks to proper fiber organization with one main direction of water molecules movement (red arrows) and low RD values (green arrow) due to the presence of physiological barriers that impede the diffusion in the perpendicular plane; (B) an injured PN demonstrates decrease of FA, related to loss of fiber organization and increase of the extracellular space with no clear directionality of water molecules movement (red arrows). Also, there is an increase of RD (green arrows) reflecting loss of myelin sheath integrity. DTI, diffusion tensor imaging; PN, peripheral nerve; FA, fractional anisotropy; RD, radial diffusivity.

neighboring structures (*Figure* 7). In cases of severe PN damage, a decrease of FA values under the determined threshold in the software for its 3D representation, may lead to an underestimation of its structure (40).

### *Plexus evaluation and degenerative disk nerve roots entrapment assessment*

Most clinical studies with DWN have been performed on brachial and lumbar plexus (17,41). In brachial plexus, DWN and DTN have demonstrated their ability to evaluate degenerative, compressive and traumatic conditions (42,43).

Brachial and lumbosacral plexus have been widely studied by DWN, in fact the first DWN sequences, described by Takahara *et al.* (10) were based on the visualization of either the brachial plexus or whole body neurography using DWIBS (diffusion-weighted imaging with background body signal suppression) (44). Brachial and lumbar plexus have also been studied by DTI. The presence of multiple interfaces between bone, fat, water and air conditions inhomogeneity of the magnetic field and suppose a challenge for the application of Echo-Planar-Imaging (EPI) sequences such as DTI, which requires strong motion gradients and the acquisition of several directions of diffusion signal. Besides, involuntary movements such as breathing, bowel loop motion, neck or abdominal vessel pulsation, swallowing or salivation can also lead to poor quality images. The use of parallel acquisition techniques or turbo-spin-echo (TSE) based DWI can help to improve the image quality.

Brachial plexus

In spite of the limitations referred above for this anatomical area, brachial plexus has been one of the most studied regions for morphological and functional neurography
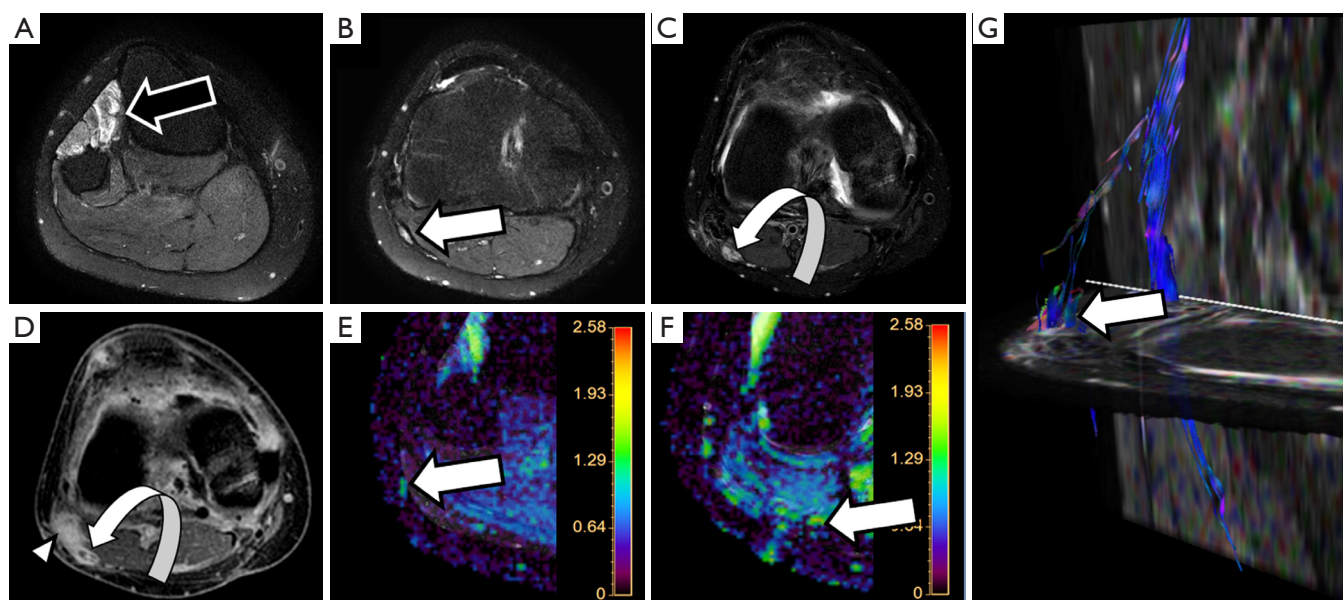
Figure 6 Evaluation of PN transection with DTI. A MRI is carried out in a 23-year-old male with previous reconstruction surgery of posterior cruciate ligament, refers weakness and impossibility for active feet dorsal flexion. (A-C) Axial SPAIR T2-weighted images demonstrate denervation signs within the anterior leg compartment (black arrow) with thickening of the distal common peroneal nerve (straight white arrow) and interruption of its visualization where it shows a nodular well-delimited appearance in vicinity of a surgical scar area (curved white arrow); (D) axial postcontrast fat suppressed T1-weighted image demonstrates peripheral enhancement of the PN lesion (curved arrow), consistent with terminal neuroma, and diffuse pseudonodular enhancement of distal biceps femoris muscle that suggest scarring tissue (arrowhead); (E,F) AD parametric maps under and above the lesion, respectively, show lower AD values of peroneal nerve below the neuroma (1.2×10^{-3} mm^2/s) in comparison to the ones above the injury (1.9×10^{-3} mm^2/s)), suggesting decrease of the normal axonal flow; (G) 3D DTI neurographic reconstruction demonstrates the absence of common peroneal nerve fibers below the neuroma (arrow) probably related to low distal FA values which conditions an underrepresentation of those nerve fibers under the same threshold value set. PN, peripheral nerves; DTI, diffusion tensor imaging; MRI, magnetic resonance imaging; SPAIR, spectral attenuated inversion recovery; AD, axial diffusivity; FA, fractional anisotropy.

applications (45,46). The prevalence of nerve root or trunk traumatic lesions at brachial plexus is much higher than in lumbosacral region and it is commonly related to direct trauma, upper limb or neck traction or torsion mechanism. Also, extrinsic compression either by degenerative disk disease at the level of the cervical spine or peripherally at the upper thoracic outlet or scalene triangle of the neck can also be found (47). Evaluation of birth-related brachial plexus injuries with MRI neurography is also raising interest due to its clinical and legal implications (48).

The avulsion of preganglionic nerve root at the cervical region after traction trauma is hard to evaluate using DWI or DTI techniques due to its small size, so they are usually studied by morphological heavily T2 weighted sequences with high resolution (49). The rest of the nerve roots and trunks can be adequately visualized both in DWI or DTI

acquisitions (45). DWI allows for a fast and comprehensive evaluation of the brachial plexus helping in the detection of traumatic plexopathy, and with a potential impact in the selection of therapeutic options (50).

Radiation induced brachial plexus damage in oncological patients is another not uncommon clinical scenario (51). In spite of new modulated radiation therapy techniques for head and neck or breast cancer treatment, post-radiotherapy brachial plexus neuropathy has to be considered when oncological patients with suspicion of brachial plexus involvement are evaluated (*Figure 8*). DWN shows nerve root thickening with increased signal intensity on high *b* values and also increase of ADC. Moreover, in these patients, DWI has the added value to rule out malignant infiltration of brachial plexus which typically shows lower ADC values with or without associated soft tissue

　　　qims.amegroups.com
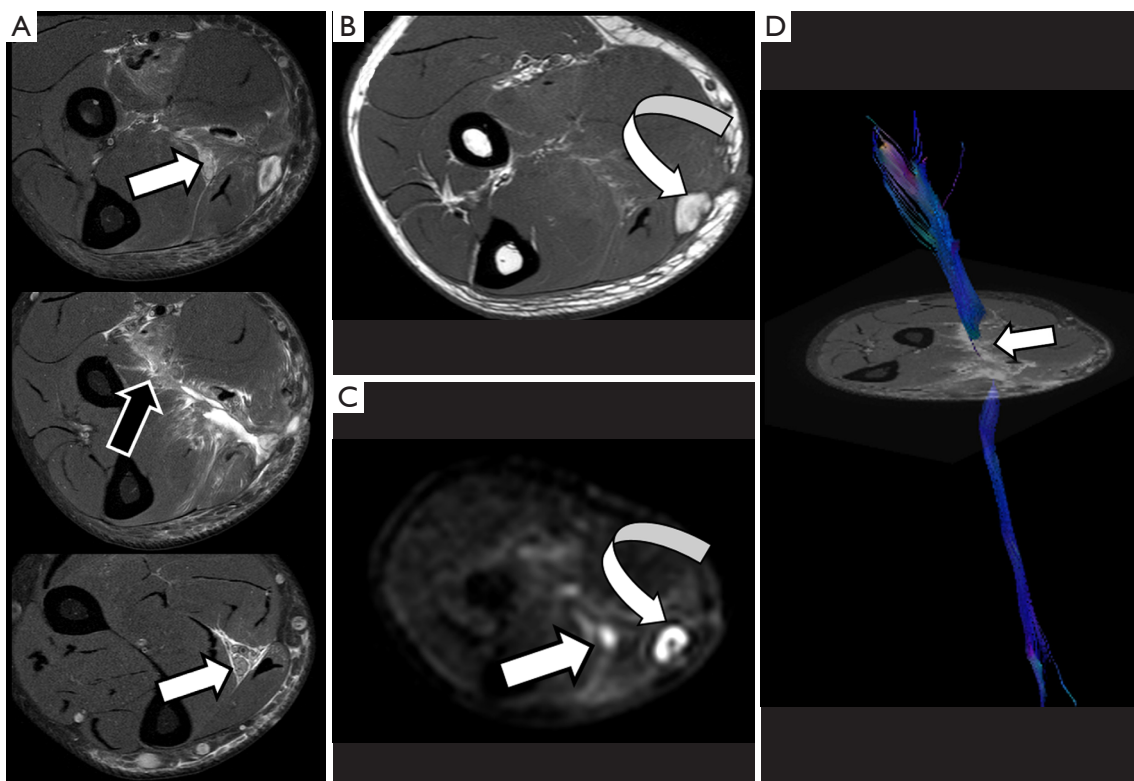
Figure 7 Evaluation with DTI of PN acute trauma. A 21-year-old male with a stab wound at forearm, who refers paresthesias and weakness at 4th and 5th fingers is studied with MRI. (A) Axial SPAIR proton-density images located below, at the level and distal to the injury site show diffuse increase of signal intensity within forearm flexor muscles (black arrow) as well as thickening of ulnar nerve (white arrows); (B) axial TSE T1-weighted image demonstrates a hemorrhagic collection close to the flexor carpi ulnaris (curved arrow); (C) axial DWI with a b value of 1,000 s/mm^2 shows an increase of signal intensity within the ulnar nerve (white arrow), representing nerve edema and increase of signal intensity within the hematoma, with peripheral low signal rim, due to susceptibility artifact (curved arrow); (D) 3D DTI neurography demonstrates absence of continuity between both segments (white arrow). DTI, diffusion tensor imaging; PN, peripheral nerves; MRI, magnetic resonance imaging; SPAIR, spectral attenuated inversion recovery; TSE, turbo-spin-echo; DWI, diffusion weighted imaging.

abnormalities. Besides, DTI through 3D neurographic reconstructions is able to demonstrate infiltration, disruption or displacement of the involved nerve roots (43).

Brachial plexus roots and trunks on DTI after a direct or an indirect trauma demonstrate similar variations of FA or RD values to those described above for PN injuries. Neuropraxia of brachial plexus roots will show a decrease of FA values, due to loss of fiber organization, and increase of RD values (*Figure 9*). The amount of these changes is directly related to the severity of the neural damage and may be consider as a complementary tool to the clinical and electrophysiological evaluation (52).

Lumbar plexus

Due to its deep location and complex anatomy, the evaluation of lumbosacral plexus by conventional ultrasound techniques or electrophysiological studies is very limited. MRI morphological and functional neurographic techniques have demonstrated high accuracy for the evaluation of this anatomical area (53). The incidence of nerve root, trunks or PN injuries at the pelvic region is usually linked to peripartum or surgical (intraoperative or postoperative) related complications. Adnexal lesions, complicated prolonged partum or gravid uterine extrinsic compression may also induce lumbosacral roots injuries, particularly involving the sciatic nerve during its course above the sacral wings or the iliac crests (54). The sciatic nerve, due to its length and course is usually involved in peripartum trauma mainly by traction or extrinsic compression mechanisms (55). DWN studies may provide useful information about the
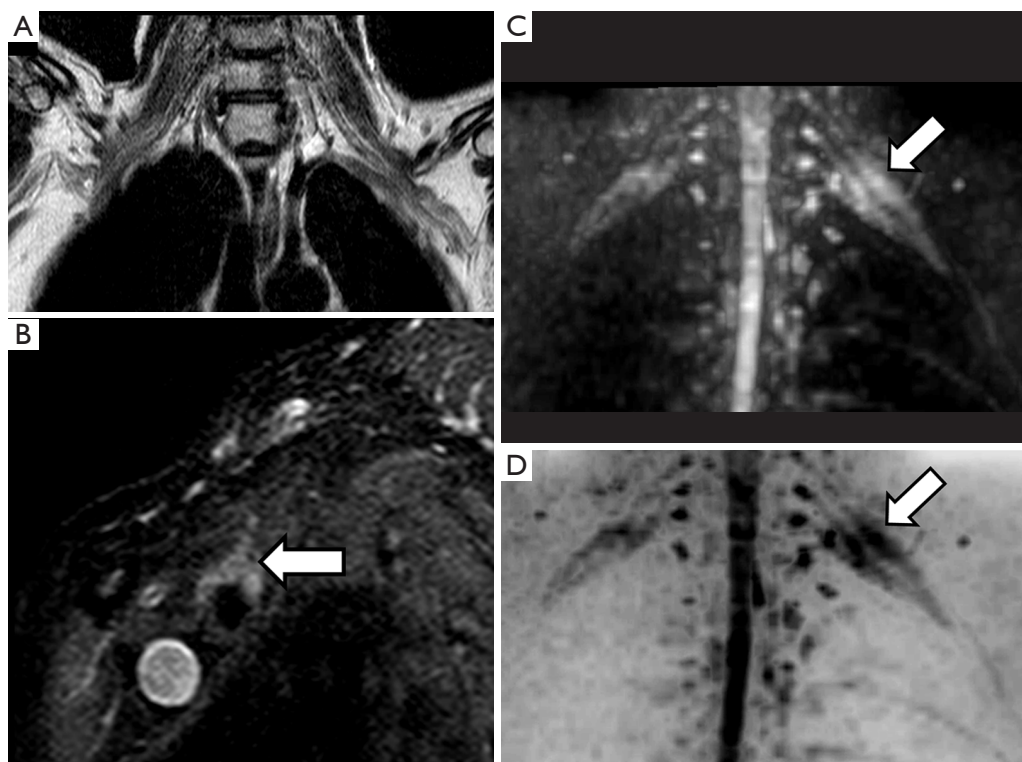
Figure 8 Brachial plexus post-radiation neuropathy. A MRI is performed in a 64-year-old female with history of radiotherapy 5 months before, as part of her treatment for left breast carcinoma, refers left arm numbness and pain. (A) Coronal TSE T2-weighted image does not reveal significant anomalies at brachial plexus trunks; (B) sagittal STIR demonstrates mild thickening of brachial plexus nerve trunks above left subclavian artery (arrow); (C,D) coronal MPR of high *b* value DWI with conventional and inverted gray scale windowing allow obtaining a neurographic view of brachial plexus, which depicts an increase of signal intensity and asymmetric thickening of left brachial plexus trunks. MRI, magnetic resonance imaging; STIR, short-tau inversion recovery; MPR, multiplanar reformation; DWI, diffusion weighted imaging.

nerve continuity and the presence of edematous changes, which can be quantified by ADC values. The most common lesion in these patients is neuropraxia, and treatment monitoring can be performed using DWN as a progressive normalization of signal intensity and decrease of ADC values will occur during the recovery of the normal nerve function (*Figure 10*). Pudendal nerve may also be involved in peripartum trauma, however, due to its small diameter is hardly identified by DWN or DTN techniques, playing a major role for its evaluation high resolution morphological sequences (56).

Compressive pathology and entrapments at lumbar spine are the other source of neuropathies in these patients, mainly related to degenerative disk disease. Specific PN entrapment, such as piriformis syndrome, will be discussed in the following section.

Derived parameters from DWN or DTN, such as ADC or FA, have proved its usefulness to identify the involved lumbar nerve roots in cases of lumbar pain (57,58). An increase in ADC and a significant decrease in FA of compressed nerve roots compared with contralateral ones are detected in cases of symptomatic lumbar disk disease. This increase of ADC values is secondary to the venous congestion and edema that occurs in both pre-ganglionic and ganglionic segments of nerve lumbar roots (41). The decrease of FA values is also related to a loss of fiber anisotropy (*Figure 11*). At this point, it is important to remember that normal preganglionic nerve roots usually show physiologically lower FA values than PN, probably due to the absence of a complete neural fiber structure. This data has to be taken into account when quantification is performed at this small nerve structure, avoiding false positive results in patients without nerve compression. This quantitative assessment shows potential to form part shortly of the clinical lumbar spine MRI protocols as a tool to detect functional changes within the lumbar
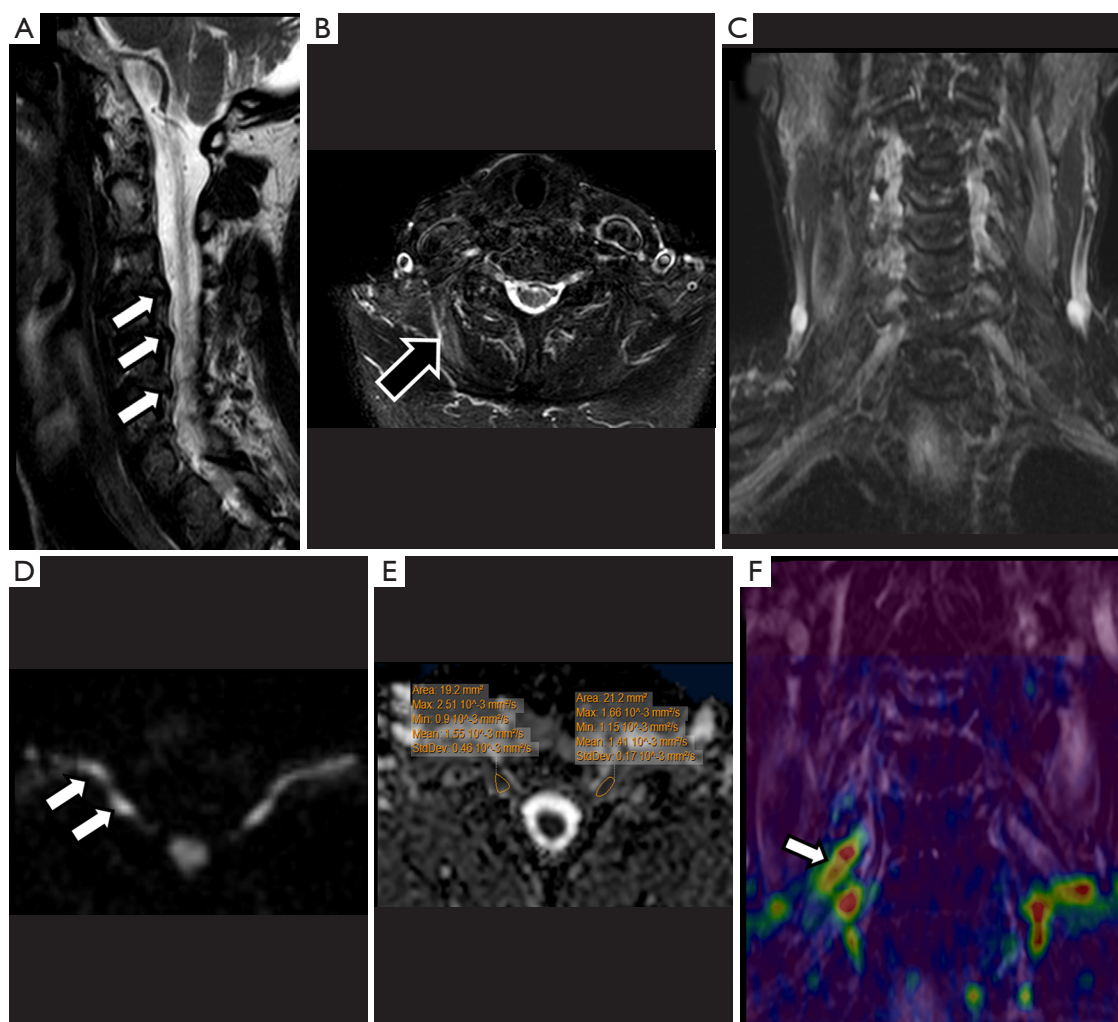
Figure 9 Assessment by DWI neurography of brachial plexus neuropraxia. A MRI is carried out in a 42-year-old female with right arm weakness and cervical pain. (A) Sagittal STIR of cervical spine shows multiple disk-osteophyte complexes (white arrows) compressing the spinal cord; (B) axial STIR at C6-C7 level demonstrates denervation signs within right splenius capitis muscle (black arrow); (C) no clear asymmetries are identified between both brachial plexus at coronal STIR neurography sequence; (D) axial DWI with a b value of 800 s/mm^2 shows higher signal intensity within right nerve root and ganglionic segment (white arrow) compared with left one; (E) ADC map demonstrated higher ADC values at right nerve root (1.55×10^{-3} mm^2/s) compared with the contralateral one (1.41×10^{-3} mm^2/s) consistent with edema; (F) fusion of morphological and functional (DWI) neurography demonstrated focal asymmetric increase of signal intensity within right C6 nerve root (arrow). DWI, diffusion weighted imaging; MRI, magnetic resonance imaging; STIR, short-tau inversion recovery; ADC, apparent diffusion coefficient.

roots in patients with symptoms but without obvious disc protrusions (41).

Peripheral nerve tunnel syndromes and entrapments

Median nerve and carpal tunnel syndrome

Assessment of the median nerve for the study of carpal tunnel syndrome has classically been a challenge for the radiologist. Numerous studies have demonstrated with proper results the utility of ultrasound (59) and conventional MRI studies to evaluate median nerve at flexor retinaculum (60). However, in some patients there is not apparent cause of median nerve compression despite the presence of clinical symptoms. It is in this group of
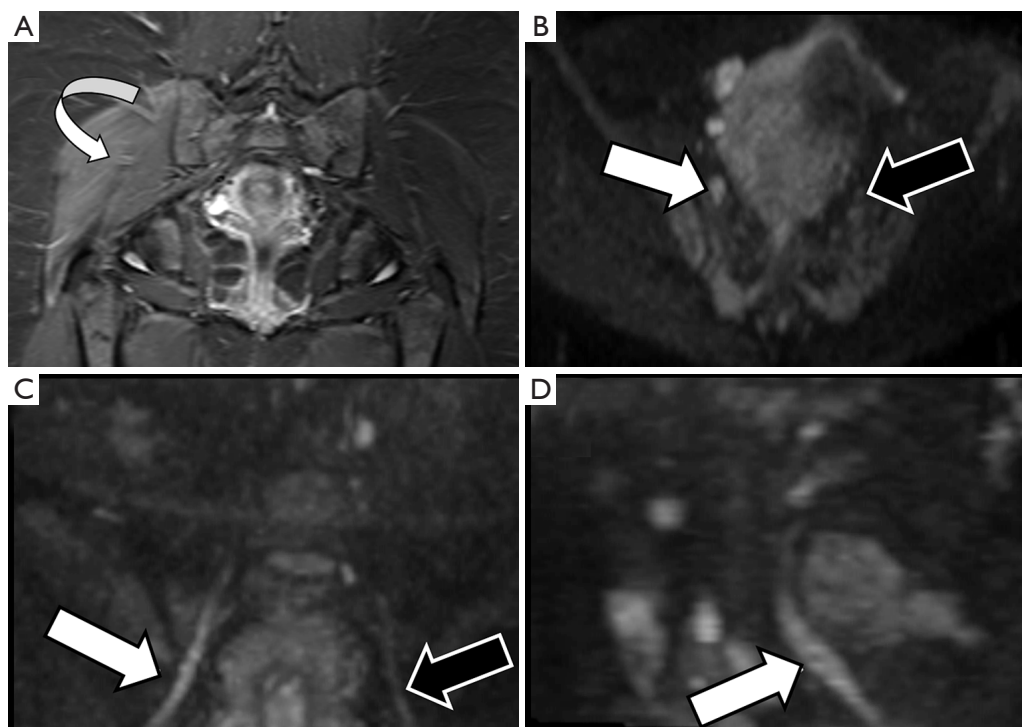
Figure 10 Partum related neuropraxia of sciatic nerve. A MRI is performed in a 32-year-old female with severe limitation of movement and deep tendon reflexes at right lower limb after prolonged partum. (A) Coronal SPAIR T2-weighted sequence shows a diffuse increase of signal intensity especially at the right gluteus medium muscle (curved arrow) without other relevant findings; (B) axial DWI study with a high b value of 800 s/mm^2 demonstrates severe thickening and hyperintensity of right sciatic nerve (white arrow) compared with left sciatic nerve (black arrow); (C,D) coronal MPR and sagittal MIP of high b value image confirm this asymmetry between both sciatic nerves and points out the relationship between right sciatic nerve (white arrow in D) and the sacral wing, as the prolonged compression of this nerve by uterus against this bone structures is the main cause of neuropraxia in this case. MRI, magnetic resonance imaging; SPAIR, spectral attenuated inversion recovery; DWI, diffusion weighted imaging; MPR, multiplanar reformation; MIP, maximum intensity projection.

patients where neurographic techniques based on DWI and DTI are showing promising results, not only in diagnosis but also in monitoring the results of surgical treatment. Median nerve has been one of the first PN deeply studied by DTI. Several studies have detailed the technical optimizations for DTN comparing healthy controls with patients with carpal tunnel syndrome (22,61,62). These studies have shown a reduction in FA values in patients with symptoms consistent with carpal tunnel syndrome, suggesting that due to compression, the median nerve loses its physiological anisotropic structure as the extracellular space increases, Also, DTN can detect long-standing neural changes (63). An increase of ADC values is also depicted due to the presence of edema (64).

The decrease of FA values has demonstrated to be more sensitive to changes in median nerve than ADC, especially at the distal carpus, after its path under the flexor retinaculum, where the most significant variation with regard to healthy volunteers is detected (63) (*Figure 12*). Other parameters such as MD, RD and AD have also been tested with promising results for carpal tunnel syndrome evaluation and with proper correlation with electrophysiological studies (5). Several cut-off points for FA values have been proposed for carpal tunnel syndrome diagnosis (65). However, differences due to technical factors such as acquisition protocols, magnet field strength (1.5 *vs.* 3.0 T), threshold FA values, reconstruction algorithms and even patient's age can act as potential bias and limit reproducibility (66). So, until a greater degree of standardization is achieved and based on the existing scientific literature, it seems reasonable to perform measures of the different parameters at least within carpal tunnel as well as at its proximal and distal segments.

In patients undergoing surgical decompression of the median nerve, DTN has also been used for assessment
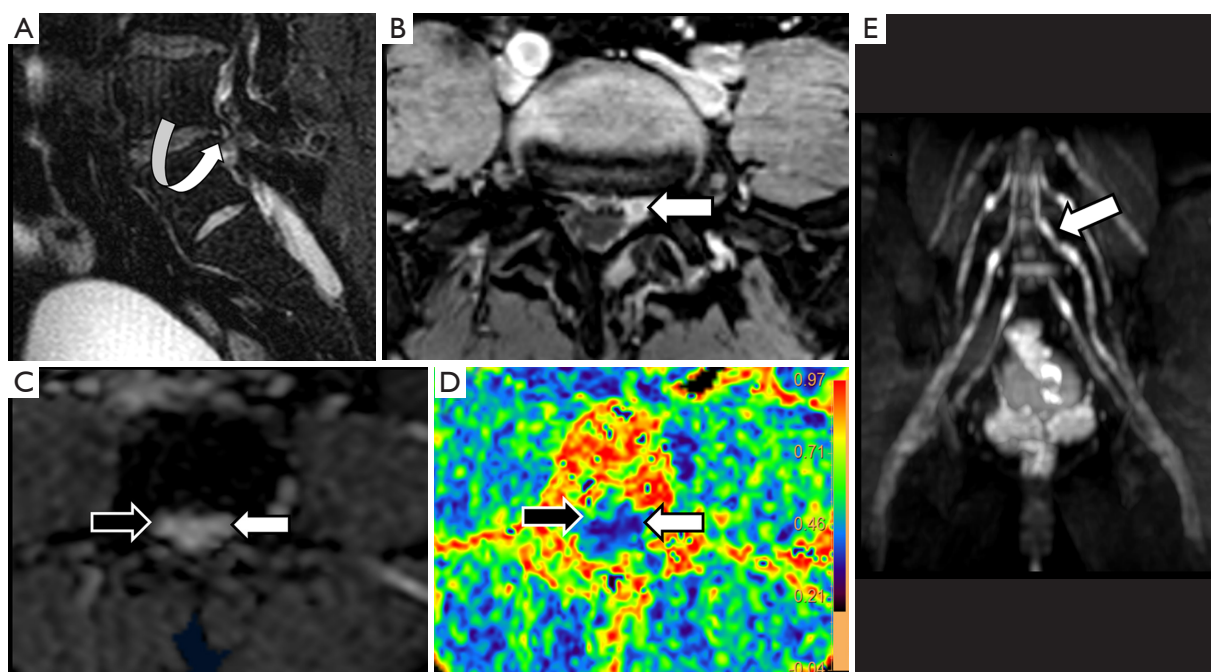

Figure 11 Lumbar root disk compression. A 56-year-old male with left sciatica is submitted to perform a MRI. (A) Sagittal STIR shows a left subarticular disk protrusion at L4–L5 level (curved arrow) that contacts with left L5 nerve root at its intracanal segment; (B) axial postcontrast THRIVE demonstrates moderate thickening and enhancement of left L5 nerve root (white arrow); (C) ADC map shows a moderate increase of ADC value at left L5 nerve root (white arrow, 1.7×10^{-3} mm^2/s) in comparison to the contralateral root (black arrow, 1.4×10^{-3} mm^2/s); (D) FA map demonstrates also a decrease of FA values at left nerve root (white arrow, 0.3) compared with right one (black arrow, 0.5). All these findings are consistent with edema and fiber disorganization due to disk compression at left L5 nerve root; (E) coronal MPR of high b value allows obtaining a neurographic view of lumbosacral plexus, which shows an increase of signal intensity of the preganglionic segment of left L5 nerve root with moderate deviation of its normal path (white arrow). MRI, magnetic resonance imaging; STIR, short-tau inversion recovery; THRIVE, T1 High-Res Isotropic Vol Excitation; ADC, apparent diffusion coefficient; FA, fractional anisotropy; MPR, multiplanar reformation.
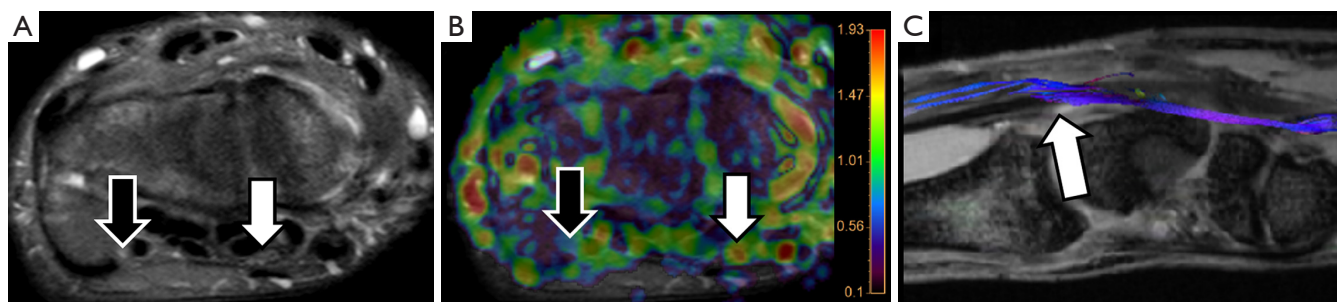
Figure 12 Carpal tunnel syndrome evaluation with DTN. Carpal tunnel syndrome in a 56-year-old female with numbness of 1st, 2nd and 3rd right hand fingers is studied with MRI. (A) Axial STIR at the flexor retinaculum level does not demonstrate any relevant alteration of neither the median nerve (white arrow) nor the ulnar nerve (black arrow); (B) fusion of axial STIR and MD color parametric map shows a moderate increase of MD values at median nerve (white arrow) within extensor retinaculum compared with ulnar nerve (black arrow) consistent with edema due to compression; (C) 3D DTI neurography depicts a slight change in angulation of median nerve path and a decrease of FA values (white arrows) suggesting focal loss of fiber integrity. DTN, DTI-neurography; MRI, magnetic resonance imaging; STIR, short-tau inversion recovery; MD, mean diffusivity; DTI, diffusion tensor imaging; FA, fractional anisotropy.
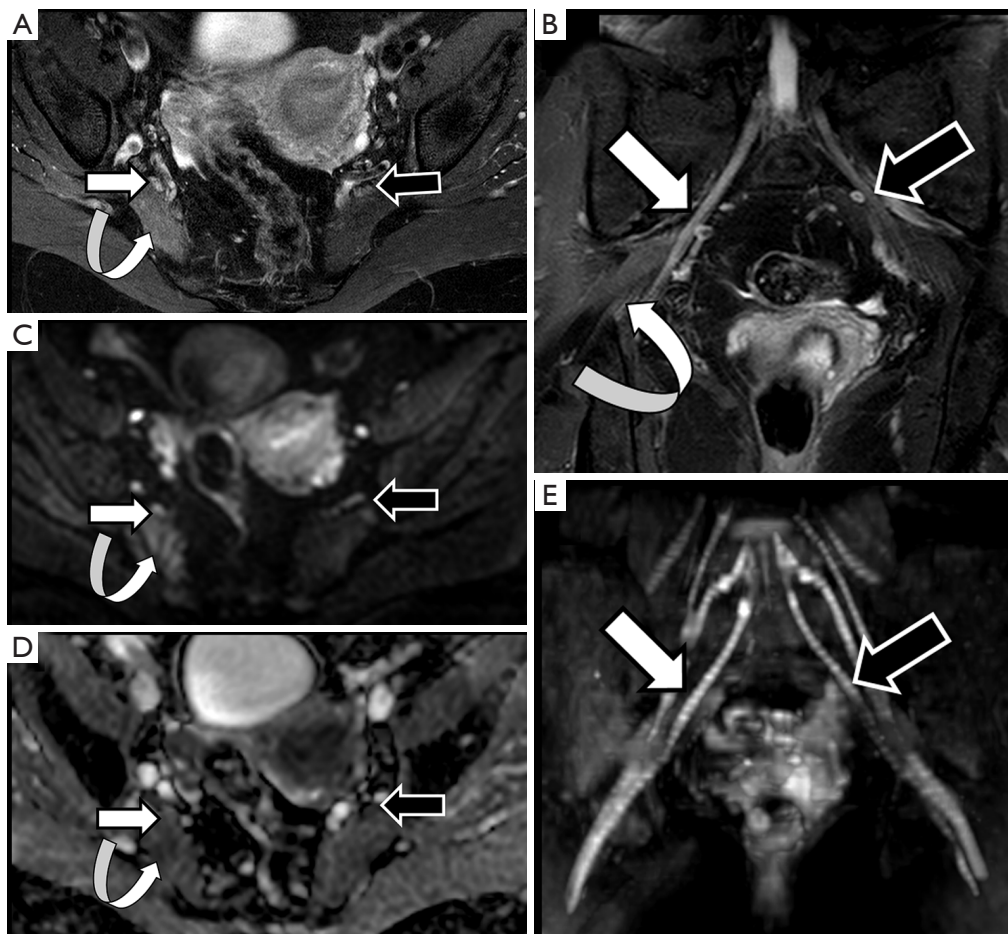
Figure 13 Piriformis syndrome assessment by DWN. (A,B) Axial and coronal SPAIR T2-weighted sequences show increase of signal intensity within right sciatic nerve (white arrow) as it crosses above piriformis muscle compared with contralateral sciatic nerve (black arrow). Note also the presence of denervation changes within the right piriformis muscle (curved arrow); (C,D) DWI study with a high *b* value of 800 s/mm^2 and corresponding ADC map demonstrate both hyperintensity of sciatic nerve (white arrows) with regard to contralateral nerve (black arrows), and also an increased ADC value of 1.8×10^{-3} mm^2/s at the right sciatic nerve in comparison to the ADC value of left sciatic nerve (1.3×10^{-3} mm^2/s) consistent with edema and increase of extracellular space at right sciatic nerve. Besides, a moderate restriction of diffusion is also seen at right piriformis muscle (curved arrows); (E) coronal MPR of high *b* value shows a neurographic view of lumbosacral plexus and lumbar roots confirming the asymmetry between both sciatic nerves. DWN, DW-based neurography; SPAIR, spectral attenuated inversion recovery; DWI, diffusion weighted imaging; ADC, apparent diffusion coefficient; MPR, multiplanar reformation.

of changes in FA before and after the intervention. It has been shown that there is a progressive increase of FA values within the first 6 weeks to 6 months after surgery in patients with clinical improvement. This increase was identified in both the proximal and distal segment of the median nerve at the wrist (67).

Sciatic nerve and piriformis syndrome

The sciatic nerve is the major PN in the body, both for its length and its width. Clinical manifestations of sciatic

nerve are common, and are challenging to study with MRI due to its length. Sciatic nerve entrapment usually occurs at a pelvic level, the so-called piriformis syndrome, due to a mass compression, trauma or a compression neuropathy (68,69). According to some authors, the existence of a piriformis hypertrophy, as may occur in runners, or accessory muscle can condition compression on the sciatic nerve and justify the symptoms (70,71). Morphological MRI is able to determine the anatomy of the piriformis muscle and its relation with the sciatic nerve, bur may not always
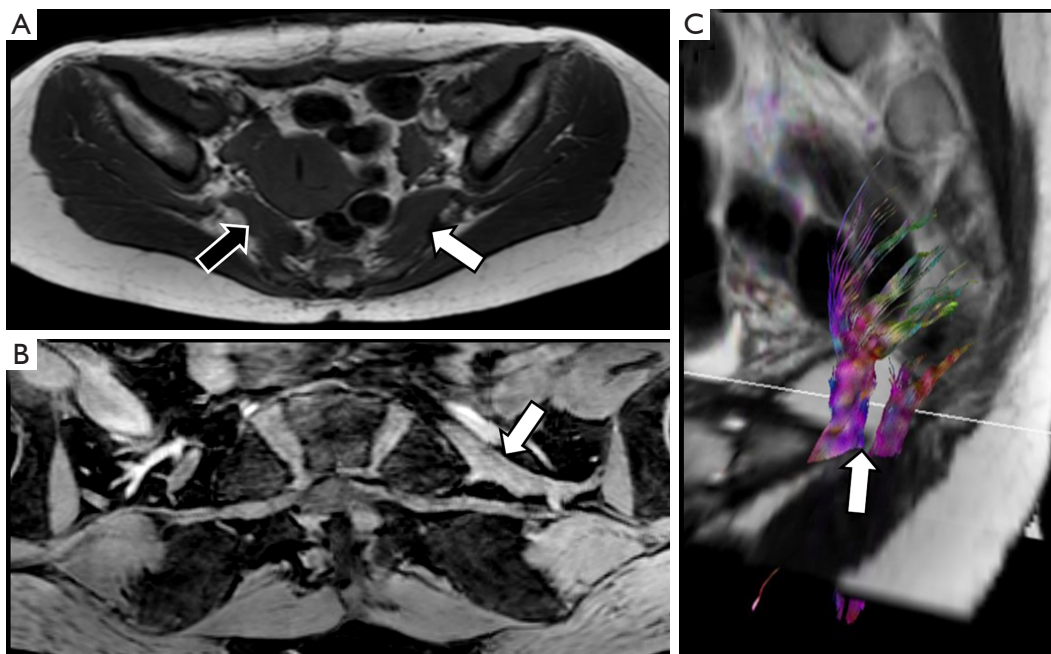
Figure 14 Piriformis syndrome evaluation with DTN. A 29-year-old female with clinical suspicious of right piriformis syndrome underwent a MRI study. (A) Axial TSE T1-weighted image shows thickening of left piriformis muscle (white arrow) in comparison to the contralateral one (black arrow); (B) MPR of THRIVE acquisition parallel to the path of both sciatic nerves identifies the presence of a left accessory piriformis muscular fascicle (white arrow); (C) DTN demonstrates the split of left sciatic nerve in two bundles (white arrow) surrounding both sides of the previously referred accessory muscular fascicle, consistent with type B variation of the classification of Beaton and Anson. DTN, DTI-neurography; MRI, magnetic resonance imaging; TSE, turbo-spin-echo; MPR, multiplanar reformation; THRIVE, T1 High-Res Isotropic Vol Excitation; DTI, diffusion tensor imaging.

show enough accuracy for detecting changes at the sciatic nerve that justify the symptoms. However, DWN allows multiplanar reconstructions that facilitate the qualitative assessment of the nerve in almost its entire length, detecting differences in signal intensity of the sciatic nerve in comparison to the contralateral, healthy one (*Figure 13*). Furthermore, at the point of nerve compression, ADC shows higher values than in the rest of the nerve, presumably due to the coexistence of edema (40,72). 3D neurographic reconstructions from DTN data may help in the assessment of the relationship between sciatic nerve and piriformis muscle and its several variants that may help clinicians to establish a most certain diagnosis of this underdiagnosed entity (73) (*Figure 14*).

Distal sciatic neuropathy with peroneal nerve compression as it crosses around the knee by extrinsic lesions or the insertion of flexor muscles is not uncommon, and functional MRI neurography may help to clarify the potential involvement of this nerve and its correlation with electrophysiological studies and clinical symptoms (*Figure 15*).

Treatment monitoring and post-surgical evaluation

Functional MRI neurography can be a useful tool to determine the diverse therapeutic options after PN trauma. Besides the assessment of nerve continuity by morphological and also functional neurographic techniques, the evaluation of the several derived parameters from DWN and DTN may help to decide further therapeutic options (74). Also, these techniques may have a potential role for *in vivo* surgery planning and selection of the segments of PN candidates for autologous nerve graft or to discard them in basis to their functional characteristics (75).

Theoretically, PN or brachial or lumbar nerve trunks with scarce decrease of FA values or minimum increase of RD values after trauma, consistent with neuropraxia, should recover *ad integrum* in a lesser time period with conservative treatment and rehabilitation than nerves with a more evident decrease of FA values and increase of RD, associated to an axonotmetic or neurotmetic injury (33). However, further studies are needed to confirm this hypothesis.
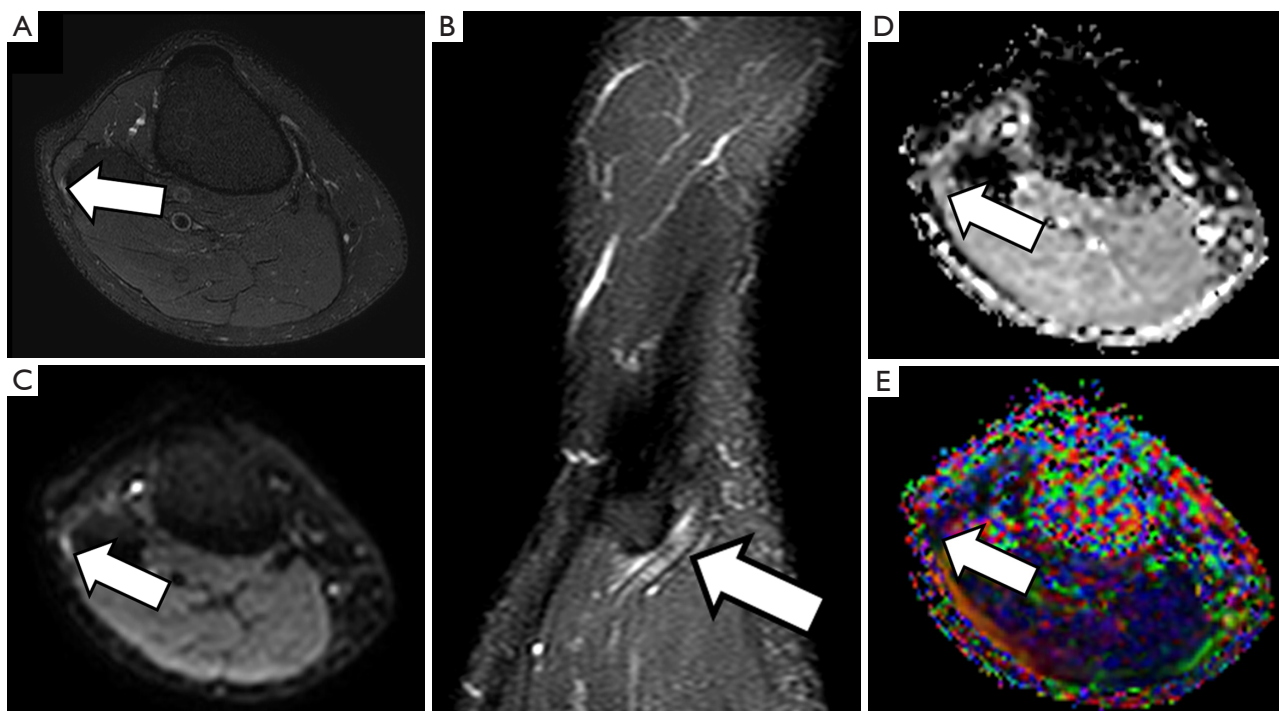
Figure 15 Common peroneal nerve neuropraxia evaluation with DTN. A 50-year-old male with right paresthesias at right lower limb after prolonged right knee flexion position was studied with a MRI. (A,B) Axial and sagittal STIR show mild increase of signal intensity of common peroneal nerve as it passes between the peroneal head and the insertion of the peroneus longus muscle; (C,D) DWI with a high b value of 800 s/mm^2 and corresponding ADC map demonstrate hyperintensity of common peroneal nerve (white arrows) with increased ADC values of 1.6×10^{-3} mm^2/s consistent with edema; (E) FA map also reveals decrease of FA values (0.3) suggesting focal loss of fiber integrity (white arrow). DTN, DTI-neurography; MRI, magnetic resonance imaging; STIR, short-tau inversion recovery; DWI, diffusion weighted imaging; ADC, apparent diffusion coefficient; FA, fractional anisotropy.

From a quantitative point of view, the regeneration process consists in a progressive increase of FA values and decrease of RD values, which reflects a remyelination and reorganization of the fascicular structure with restoration of the normal anisotropic configuration of PN, thanks to the ability of PN axons to grow and regenerate after their section (76-78). Also, ADC and MD values will normalize due to the decrease of edema within the nerve and surrounding structures (79). For all these reasons, derived parameters from DWN or DTN may be considered in a near future as biomarkers and potential predictors of the outcome of this type of patients.

In those PN or trunks with more severe neural damage indicated by FA or RD, or with no functional (motor, sensitive or quantitative) recovery after 3 months of conservative treatment, a surgical approach may be considered. It is out of the aim of this paper to enumerate or detail the different surgical techniques for PN injuries

treatment. However, it is important to recognize the post-surgical changes that can be found in control studies and the potential role of functional MRI neurography for their evaluation (80).

Neurolysis, neurorrhaphy using nylon suture or fibrin glue, as well as autologous nerve graft have the goal of restoring the nerve continuity and thus, its axonal flow and function (75). DWI and DTI are sequences prone to suffer from susceptibility artifacts. Suture material or blood products, especially in the first weeks after surgery, used for PN reconstruction may condition important local magnetic field inhomogeneities that would cause image distortion or poor quality and inaccurate parametric maps. To the best of our knowledge, no studies have previously evaluated the potential limitation or interference caused by these external materials at the surgery site for DWN or DTN evaluation. We recommend to evaluate also the proximal and distal segments, where the quantification of the diverse
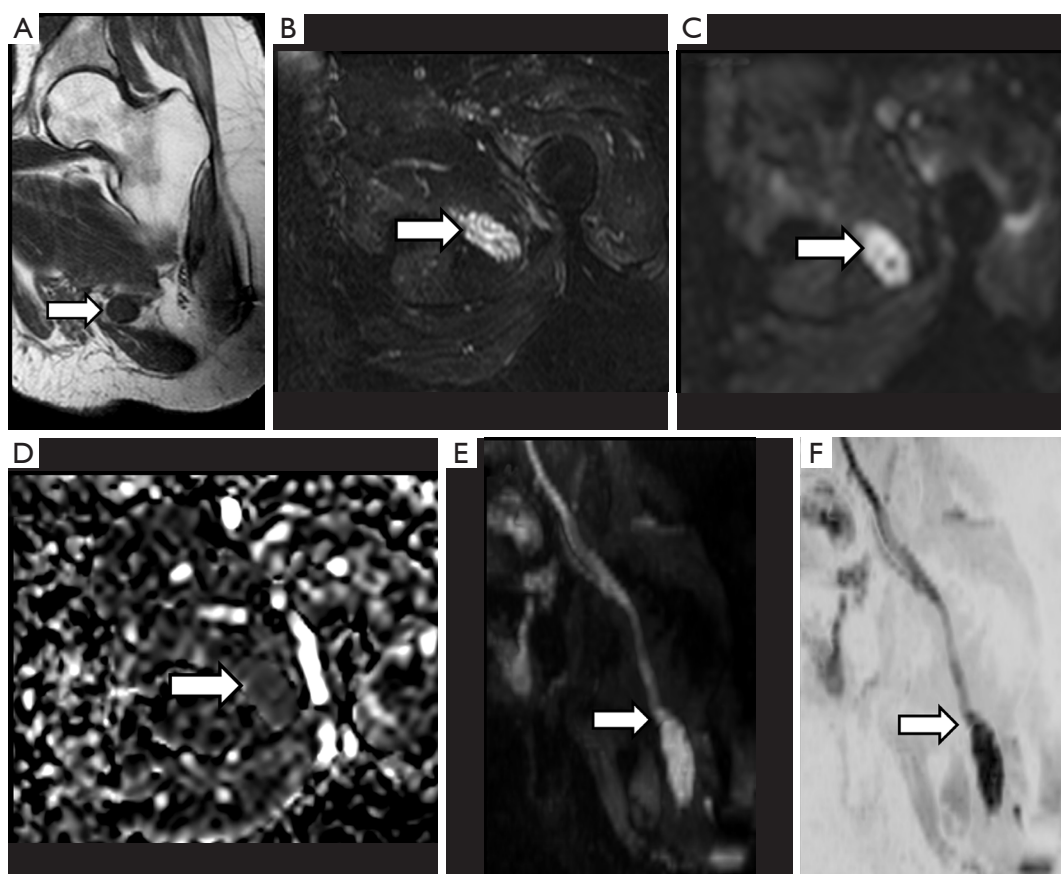

Figure 16 Terminal neuroma. A 34-year-old male with soft tissue sarcoma at proximal thigh was studied with MRI. A nodular lesion is identified at morphological sequences. (A) Coronal TSE T1-weighted image and (B) axial STIR show a focal lesion in the vicinity of surgical scar tissue (white arrow) that forces to rule out malignancy recurrence; (C,D) DWN study with a high b value of 800 s/mm^2 and corresponding ADC map demonstrate moderate restriction of water diffusion within this lesion, with ADC value of 1.3×10^{-3} mm^2/s consistent with a benign nature (white arrow); (E,F) coronal MPR of the high b value presented with conventional grey scale and inverted one, respectively, allow obtaining a neurographic view of the whole course of left sciatic nerve demonstrating both morphological and functional continuity and dependence of the suspicious lesion with the nerve (white arrows), being consistent, with amputation or terminal neuroma. MRI, magnetic resonance imaging; TSE, turbo-spin-echo; DWN, DWI-neurography; ADC, apparent diffusion coefficient; MPR, multiplanar reformation.

parameters should be more reliable.

After surgical repair, FA values should progressively increase at the distal site of the nerve injury reflecting restoration of nerve continuity. Changes in RD may depend on the severity of the previous nerve trauma, which may induce distal nerve damage due to the disruption of vasa nervorum. In this field, the recovery (with increase) of AD values at the distal segment would be a potential biomarker of axonal flow restoration. However, further studies are needed to confirm the usefulness of this approach. DTN studies may also assess the existence of growing neural

fibers during the regeneration process (80).

One of the most characteristic lesions associated to previous surgery are neuromas. These lesions may appear at the proximal terminal edge of PN after a total nerve section, which is the rule after limb amputations or total transections without surgical repair. Other neuromas usually appear around surgical sutures or tissue scars in the continuity of the nerve path, or after a traction injury of PN. These neuromas usually appear in DWN studies as hyperintense structures at high b values with low ADC values usually between 1.1 and 1.2×10^{-3} mm^2/s (20). Neuromas are a solid
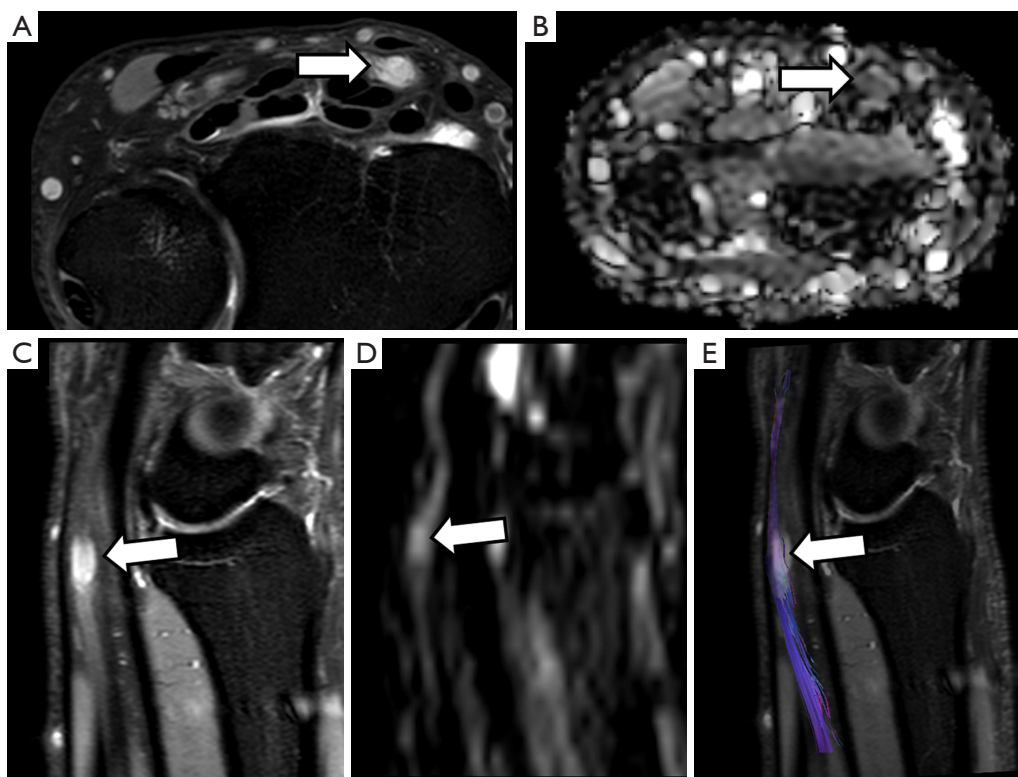
Figure 17 Median nerve continuity neuroma evaluation with DTN. A MRI is performed in a 45-year-old male with stab injury at the palmar surface of the distal forearm that refers paresthesias at 1st and 2nd fingers. (A) Axial SPAIR proton-density image shows focal thickening and a nodular lesion at median nerve (white arrow) at the same site of the previous stab injury; (B) ADC map demonstrates low ADC values (1.1×10^{-3} mm^2/s) of this lesion (white arrow); (C) sagittal SPIR T2-weighted; (D) MPR in sagittal plane of high *b* value DWI and (E) 3D DTI neurographic reconstruction demonstrate morphological and functional continuity between the lesion and the median nerve (white arrows), findings consistent with neuroma-in-continuity. DTN, DTI-neurography; MRI, magnetic resonance imaging; SPAIR, spectral attenuated inversion recovery; ADC, apparent diffusion coefficient; MPR, multiplanar reformation; DWI, diffusion weighted imaging; DTI, diffusion tensor imaging.

lesion with decrease of extracellular space, leading on less freedom of water molecules movement (*Figure 16*). Thus, DWI may help in an easy and fast manner within a single exam to establish both morphological and functional continuity between the neuroma and the rest of the PN and to characterize, in basis of its ADC values, the lesion as a benign tumor related to previous surgery or trauma. Neurofibromas may show similar ADC values than neuromas, but without previous history of PN trauma or surgery. Neuromas show lower FA values than the rest of the nerve due to absence of fiber organization. DTN and derived 3D neurographic reconstructions may help to demonstrate the dependence or continuity of neuromas within the rest of the PN (*Figure 17*).

Hematomas, seromas and abscesses are other kind of lesions that can be found at the surgical bed. Abscesses will appear hyperintense on DWI with very low ADC values due to the presence of pus and debris that conditions water diffusion restriction. Moreover, the typical appearance of these lesions at morphological MRI sequences can also help to narrow this differential diagnosis.

Fibrotic changes after PN nerve trauma or surgery, usually involve the suture place and condition a retraction, thickening or irregularity of the nerve that has undergone surgical repair. Fibrosis may interfere with the normal axonal conduction and distort the normal PN shape with decrease of FA values, both at the suture place and also distally. However, large multicenter studies are needed to confirm these possible applications. 3D neurographic reconstructions from DTI may also allow evaluating the
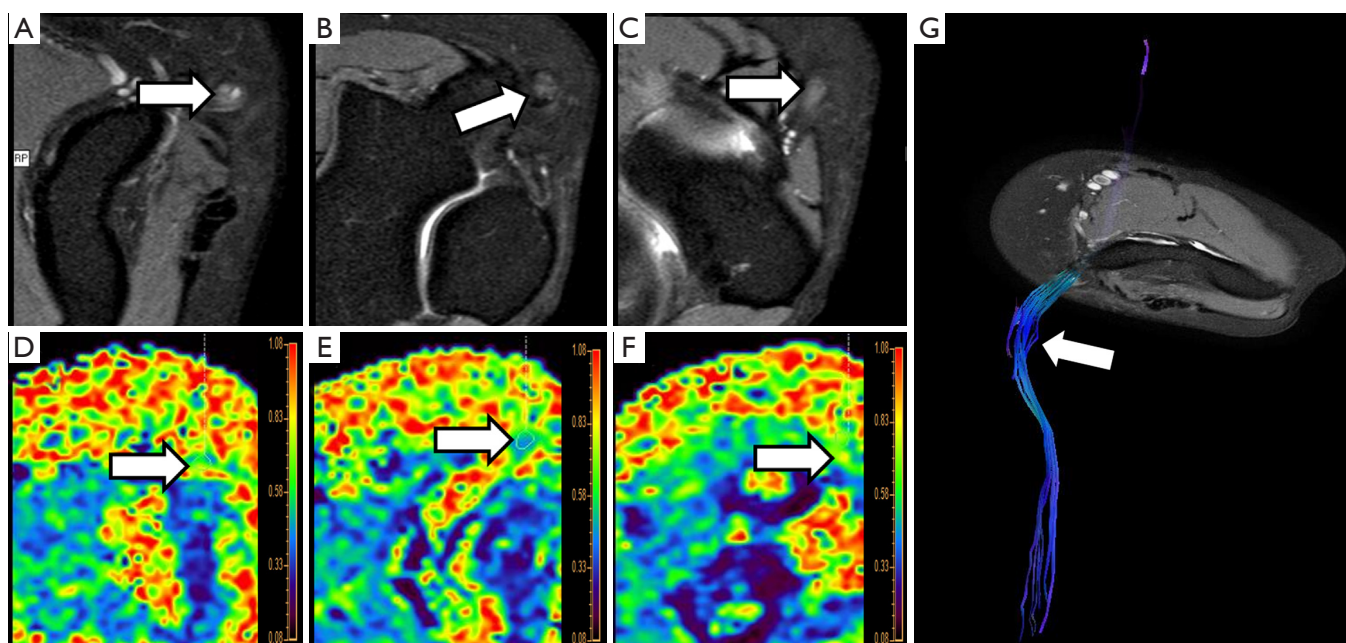
Figure 18 Assessment with DTN of incomplete release of ulnar nerve. A 46-year-old female with sporadic numbness of 4th and 5th fingers after ulnar nerve surgery is submitted to a MRI. (A-C) Axial SPAIR proton-density images at the level of proximal ulnar tunnel, epitrochlear and distal ulnar tunnel, respectively, show moderate thickening and increase of signal intensity of ulnar nerve, which is more conspicuous at the inlet and epitrochlear levels; (D-F) consecutive FA maps at the same levels than (A-C) demonstrate decrease of FA values, particularly at the level of the epitrochlear (0.33) with normalization of FA values distally to ulnar tunnel (0.45); (G) 3D DTI neurographic reconstruction demonstrates continuity of ulnar nerve with partial loss of fiber integrity at the epitrochlear level (arrow). DTN, DTI-neurography; MRI, magnetic resonance imaging; SPAIR, spectral attenuated inversion recovery; FA, fractional anisotropy; DTI, diffusion tensor imaging.

integrity and displacement of the sutured nerve (*Figure 18*).

Conclusions

DTI and DWI neurographic studies provide both valuable morphological and functional information in several clinical scenarios, that helps to understand the different pathophysiological process that occurs in PN injury related lesions. Parametric data derived from these sequences add quantitative information to PN study, helping in the detection and characterization of neural damage and grading its severity. Besides, these data can help to determine the most appropriate therapeutic option, as well as to monitoring the response to conservative or surgical treatment. In spite of the time penalty, the introduction of these techniques in routine MRI protocols for PN injury evaluation should be strongly considered. However, further prospective multicenter studies are needed to confirm parameters such as FA or RD as real biomarkers of neural damage. Finally, the standardization of both the acquisition and analysis protocols is key to obtain more reproducible and robust results.

Footnote

Conflicts of Interest: The authors have no conflicts of interest to declare.

References

1. Marquez Neto OR, Leite MS, Freitas T, Freitas T, Mendelovitz P, Villela EA, Kessler IM. The role of magnetic resonance imaging in the evaluation of peripheral nerves following traumatic lesion: where do we stand? Acta Neurochir (Wien) 2017;159:281-90.

2. Pham M, Bäumer T, Bendszus M. Peripheral nerves and plexus: imaging by MR-neurography and high-resolution ultrasound. Curr Opin Neurol 2014;27:370-9.

3. Kästel T, Heiland S, Bäumer P, Bartsch AJ, Bendszus M, Pham M. Magic angle effect: a relevant artifact in MR neurography at 3T? AJNR Am J Neuroradiol 2011;32:821-7.

4. Martín Noguerol T, Martínez Barbero JP. Advanced diffusion MRI and biomarkers in the central nervous system: a new approach. Radiologia 2017;59:273-85.

5. Heckel A, Weiler M, Xia A, Ruetters M, Pham M, Bendszus M, Heiland S, Baeumer P. Peripheral Nerve Diffusion Tensor Imaging: Assessment of Axon and Myelin Sheath Integrity. PLoS One 2015;10:e0130833.

6. Chhabra A, Thakkar RS, Andreisek G, Chalian M, Belzberg AJ, Blakeley J, Hoke A, Thawait GK, Eng J, Carrino JA. Anatomic MR imaging and functional diffusion tensor imaging of peripheral nerve tumors and tumorlike conditions. AJNR Am J Neuroradiol 2013;34:802-7.

7. Skorpil M, Engström M, Nordell A. Diffusion-direction-dependent imaging: a novel MRI approach for peripheral nerve imaging. Magn Reson Imaging 2007;25:406-11.

8. Zhao L, Wang G, Yang L, Wu L, Lin X, Chhabra A. Diffusion-weighted MR neurography of extremity nerves with unidirectional motion-probing gradients at 3 T: feasibility study. AJR Am J Roentgenol 2013;200:1106-14.

9. Takahara T, Hendrikse J, Kwee TC, Yamashita T, Van Cauteren M, Polders D, Boer V, Imai Y, Mali WP, Luijten PR. Diffusion-weighted MR neurography of the sacral plexus with unidirectional motion probing gradients. Eur Radiol 2010;20:1221-6.

10. Takahara T, Hendrikse J, Yamashita T, Mali WP, Kwee TC, Imai Y, Luijten PR. Diffusion-weighted MR neurography of the brachial plexus: feasibility study. Radiology 2008;249:653-60.

11. Eguchi Y, Ohtori S, Yamashita M, Yamauchi K, Suzuki M, Orita S, Kamoda H, Arai G, Ishikawa T, Miyagi M, Ochiai N, Kishida S, Masuda Y, Ochi S, Kikawa T, Takaso M, Aoki Y, Toyone T, Suzuki T, Takahashi K. Clinical applications of diffusion magnetic resonance imaging of the lumbar foraminal nerve root entrapment. Eur Spine J 2010;19:1874-82.

12. Eppenberger P, Andreisek G, Chhabra A. Magnetic resonance neurography: diffusion tensor imaging and future directions. Neuroimaging Clin N Am 2014;24:245-56.

13. Brandão LA, Shiroishi MS, Law M. Brain tumors:

a multimodality approach with diffusion-weighted imaging, diffusion tensor imaging, magnetic resonance spectroscopy, dynamic susceptibility contrast and dynamic contrast-enhanced magnetic resonance imaging. Magn Reson Imaging Clin N Am 2013;21:199-239.

14. Mukherjee P. Diffusion tensor imaging and fiber tractography in acute stroke. Neuroimaging Clin N Am 2005;15:655-65, xii.

15. Yoon H, Kim J, Moon WJ, Nahm SS, Zhao J, Kim HM, Eom K. Characterization of Chronic Axonal Degeneration Using Diffusion Tensor Imaging in Canine Spinal Cord Injury: A Quantitative Analysis of Diffusion Tensor Imaging Parameters According to Histopathological Differences. J Neurotrauma 2017. [Epub ahead of print].

16. de Figueiredo EH, Borgonovi AF, Doring TM. Basic concepts of MR imaging, diffusion MR imaging, and diffusion tensor imaging. Magn Reson Imaging Clin N Am 2011;19:1-22.

17. Mallouhi A, Marik W, Prayer D, Kainberger F, Bodner G, Kasprian G. 3T MR tomography of the brachial plexus: structural and microstructural evaluation. Eur J Radiol 2012;81:2231-45.

18. Chhabra A, Andreisek G, Soldatos T, Wang KC, Flammang AJ, Belzberg AJ, Carrino JA. MR neurography: past, present, and future. AJR Am J Roentgenol 2011;197:583-91.

19. Anderson AW, Xie J, Pizzonia J, Bronen RA, Spencer DD, Gore JC. Effects of cell volume fraction changes on apparent diffusion in human cells. Magn Reson Imaging 2000;18:689-95.

20. Ahlawat S, Chhabra A, Blakely J. Magnetic resonance neurography of peripheral nerve tumors and tumorlike conditions. Neuroimaging Clin N Am 2014;24:171-92.

21. Provenzale JM, Isaacson J, Chen S, Stinnett S, Liu C. Correlation of apparent diffusion coefficient and fractional anisotropy values in the developing infant brain. AJR Am J Roentgenol 2010;195:W456-62.

22. Guggenberger R, Markovic D, Eppenberger P, Chhabra A, Schiller A, Nanz D, Prüssmann K, Andreisek G. Assessment of median nerve with MR neurography by using diffusion-tensor imaging: normative and pathologic diffusion values. Radiology 2012;265:194-203.

23. Papanikolaou N, Karampekios S, Papadaki E, Malamas M, Maris T, Gourtsoyiannis N. Fractional anisotropy and mean diffusivity measurements on normal human brain: comparison between low-and high-resolution diffusion tensor imaging sequences. Eur Radiol. 2006;16:187-92.

24. Wheeler-Kingshott CA, Cercignani M. About "axial" and

"radial" diffusivities. Magn Reson Med 2009;61:1255-60.

25. Breckwoldt MO, Stock C, Xia A, Heckel A, Bendszus M, Pham M, Heiland S, Bäumer P. Diffusion Tensor Imaging Adds Diagnostic Accuracy in Magnetic Resonance Neurography. Invest Radiol 2015;50:498-504.

26. Mathys C, Aissa J, Meyer Zu Hörste G, Reichelt DC, Antoch G, Turowski B, Hartung HP, Sheikh KA, Lehmann HC. Peripheral neuropathy: assessment of proximal nerve integrity by diffusion tensor imaging. Muscle Nerve 2013;48:889-96.

27. Lehmann HC, Zhang J, Mori S, Sheikh KA. Diffusion tensor imaging to assess axonal regeneration in peripheral nerves. Exp Neurol 2010;223:238-44.

28. Filler A. Magnetic resonance neurography and diffusion tensor imaging: origins, history, and clinical impact of the first 50,000 cases with an assessment of efficacy and utility in a prospective 5000-patient study group. Neurosurgery 2009;65:A29-43.

29. Quinn JC, Fruauff K, Lebl DR, Giambrone A, Cammisa FP, Gupta A, Chazen JL. Magnetic Resonance Neurography of the Lumbar Plexus at the L4-L5 Disc: Development of a Preoperative Surgical Planning Tool for Lateral Lumbar Transpsoas Interbody Fusion (LLIF). Spine (Phila Pa 1976) 2015;40:942-7.

30. Schwarz D, Weiler M, Pham M, Heiland S, Bendszus M, Bäumer P. Diagnostic signs of motor neuropathy in MR neurography: nerve lesions and muscle denervation. Eur Radiol 2015;25:1497-503.

31. Dong Q, Welsh RC, Chenevert TL, Carlos RC, Maly-Sundgren P, Gomez-Hassan DM, Mukherji SK. Clinical applications of diffusion tensor imaging. J Magn Reson Imaging 2004;19:6-18.

32. Lindberg PG, Sanchez K, Ozcan F, Rannou F, Poiraudeau S, Feydy A, Maier MA. Correlation of force control with regional spinal DTI in patients with cervical spondylosis without signs of spinal cord injury on conventional MRI. Eur Radiol 2016;26:733-42.

33. Menorca RM, Fussell TS, Elfar JC. Nerve physiology: mechanisms of injury and recovery. Hand Clin 2013;29:317-30.

34. Seddon HJ. A Classification of Nerve Injuries. Br Med J 1942;2:237-9.

35. Sunderland S. Rate of regeneration of sensory nerve fibers. Arch Neurol Psychiatry 1947;58:1-6.

36. Morisaki S, Kawai Y, Umeda M, Nishi M, Oda R, Fujiwara H, Yamada K, Higuchi T, Tanaka C, Kawata M, Kubo T. In vivo assessment of peripheral nerve regeneration by diffusion tensor imaging. J Magn Reson Imaging

2011;33:535-42.

37. Pham M, Wessig C, Brinkhoff J, Reiners K, Stoll G, Bendszus M. MR neurography of sciatic nerve injection injury. J Neurol 2011;258:1120-5.

38. Mac Donald CL, Dikranian K, Bayly P, Holtzman D, Brody D. Diffusion tensor imaging reliably detects experimental traumatic axonal injury and indicates approximate time of injury. J Neurosci 2007;27:11869-76.

39. Stanisz GJ, Midha R, Munro CA, Henkelman RM. MR properties of rat sciatic nerve following trauma. Magn Reson Med 2001;45:415-20.

40. Li X, Chen J, Hong G, Sun C, Wu X, Peng MJ, Zeng G. In vivo DTI longitudinal measurements of acute sciatic nerve traction injury and the association with pathological and functional changes. Eur J Radiol 2013;82:e707-14.

41. Eguchi Y, Ohtori S, Yamashita M, Yamauchi K, Suzuki M, Orita S, Kamoda H, Arai G, Ishikawa T, Miyagi M, Ochiai N, Kishida S, Inoue G, Masuda Y, Ochi S, Kikawa T, Toyone T, Takaso M, Aoki Y, Takahashi K. Diffusion-weighted magnetic resonance imaging of symptomatic nerve root of patients with lumbar disk herniation. Neuroradiology 2011;53:633-41.

42. Tagliafico A, Calabrese M, Puntoni M, Pace D, Baio G, Neumaier CE, Martinoli C. Brachial plexus MR imaging: accuracy and reproducibility of DTI-derived measurements and fibre tractography at 3.0-T. Eur Radiol 2011;21:1764-71.

43. Vargas MI, Viallon M, Nguyen D, Delavelle J, Becker M. Diffusion tensor imaging (DTI) and tractography of the brachial plexus: feasibility and initial experience in neoplastic conditions. Neuroradiology 2010;52:237-45.

44. Yamashita T, Kwee TC, Takahara T. Whole-body magnetic resonance neurography. N Engl J Med 2009;361:538-9.

45. Ho MJ, Manoliu A, Kuhn FP, Stieltjes B, Klarhöfer M, Feiweier T, Marcon M, Andreisek G. Evaluation of Reproducibility of Diffusion Tensor Imaging in the Brachial Plexus at 3.0 T. Invest Radiol 2017;52:482-7.

46. Lutz AM, Gold G, Beaulieu C. MR imaging of the brachial plexus. Neuroimaging Clin N Am 2014;24:91-108.

47. Upadhyaya V, Upadhyaya DN, Kumar A, Gujral RB. MR neurography in traumatic brachial plexopathy. Eur J Radiol 2015;84:927-32.

48. Smith AB, Gupta N, Strober J, Chin C. Magnetic resonance neurography in children with birth-related brachial plexus injury. Pediatr Radiol 2008;38:159-63.

49. Gasparotti R, Ferraresi S, Pinelli L, Crispino M, Pavia M, Bonetti M, Garozzo D, Manara O, Chiesa

A. Three-dimensional MR myelography of traumatic injuries of the brachial plexus. AJNR Am J Neuroradiol 1997;18:1733-42.

50. Fisher S, Wadhwa V, Manthuruthil C, Cheng J, Chhabra A. Clinical impact of magnetic resonance neurography in patients with brachial plexus neuropathies. Br J Radiol 2016;89:20160503.

51. Cai Z, Li Y, Hu Z, Fu R, Rong X, Wu R, Cheng J, Huang X, Luo J, Tang Y. Radiation-induced brachial plexopathy in patients with nasopharyngeal carcinoma: a retrospective study. Oncotarget 2016;7:18887-95.

52. Schwarz D, Pedro MT, Brand C, Bendszus M, Antoniadis G. Nerve injuries and traumatic lesions of the brachial plexus: Imaging diagnostics and therapeutic options. Radiologe 2017;57:184-94.

53. Delaney H, Bencardino J, Rosenberg ZS. Magnetic resonance neurography of the pelvis and lumbosacral plexus. Neuroimaging Clin N Am 2014;24:127-50.

54. Fonti Y, Giordano R, Cacciatore A, Romano M, La Rosa B. Post partum pelvic floor changes. J Prenat Med 2009;3:57-9.

55. Robbins NM, Shah V, Benedetti N, Talbott JF, Chin CT, Douglas VC. Magnetic resonance neurography in the diagnosis of neuropathies of the lumbosacral plexus: a pictorial review. Clin Imaging 2016;40:1118-30.

56. Wadhwa V, Hamid AS, Kumar Y, Scott KM, Chhabra A. Pudendal nerve and branch neuropathy: magnetic resonance neurography evaluation. Acta Radiol 2017;58:726-33.

57. Budzik JF, Verclytte S, Lefebvre G, Monnet A, Forzy G, Cotten A. Assessment of reduced field of view in diffusion tensor imaging of the lumbar nerve roots at 3 T. Eur Radiol 2013;23:1361-6.

58. Miyagi R, Sakai T, Yamabe E, Yoshioka H. Consecutive assessment of FA and ADC values of normal lumbar nerve roots from the junction of the dura mater. BMC Musculoskelet Disord 2015;16:156.

59. Fowler JR, Gaughan JP, Ilyas AM. The sensitivity and specificity of ultrasound for the diagnosis of carpal tunnel syndrome: a meta-analysis. Clin Orthop Relat Res 2011;469:1089-94.

60. Jarvik JG, Yuen E, Haynor DR, Bradley CM, Fulton-Kehoe D, Smith-Weller T, Wu R, Kliot M, Kraft G, Wang L, Erlich V, Heagerty PJ, Franklin GM. MR nerve imaging in a prospective cohort of patients with suspected carpal tunnel syndrome. Neurology 2002;58:1597-602.

61. Guggenberger R, Eppenberger P, Markovic D, Nanz D, Chhabra A, Pruessmann KP, Andreisek G. MR

neurography of the median nerve at 3.0T: optimization of diffusion tensor imaging and fiber tractography. Eur J Radiol 2012;81:e775-82.

62. Meek MF, Stenekes MW, Hoogduin HM, Nicolai JP. In vivo three-dimensional reconstruction of human median nerves by diffusion tensor imaging. Exp Neurol 2006;198:479-82.

63. Barcelo C, Faruch M, Lapègue F, Bayol MA, Sans N. 3-T MRI with diffusion tensor imaging and tractography of the median nerve. Eur Radiol 2013;23:3124-30.

64. Wang CK, Jou IM, Huang HW, Chen PY, Tsai HM, Liu YS, Lin CC. Carpal tunnel syndrome assessed with diffusion tensor imaging: comparison with electrophysiological studies of patients and healthy volunteers. Eur J Radiol 2012;81:3378-83.

65. Wang H, Ma J, Zhao L, Wang Y, Jia X. Utility of MRI Diffusion Tensor Imaging in Carpal Tunnel Syndrome: A Meta-Analysis. Med Sci Monit 2016;22:736-42.

66. Hiltunen J, Kirveskari E, Numminen J, Lindfors N, Göransson H, Hari R. Pre- and post-operative diffusion tensor imaging of the median nerve in carpal tunnel syndrome. Eur Radiol 2012;22:1310-9.

67. Naraghi A, da Gama Lobo L, Menezes R, Khanna M, Sussman M, Anastakis D, White LM. Diffusion tensor imaging of the median nerve before and after carpal tunnel release in patients with carpal tunnel syndrome: feasibility study. Skeletal Radiol 2013;42:1403-12.

68. Lewis AM, Layzer R, Engstrom JW, Barbaro NM, Chin CT. Magnetic resonance neurography in extraspinal sciatica. Arch Neurol 2006;63:1469-72.

69. Hernando MF, Cerezal L, Pérez-Carro L, Abascal F, Canga A. Deep gluteal syndrome: anatomy, imaging, and management of sciatic nerve entrapments in the subgluteal space. Skeletal Radiol 2015;44:919-34.

70. Beaton LE, Anson BJ. The relation of the sciatic nerve and of its subdivisions to the piriformis muscle. Anat Rec 1937;70:1-5.

71. Varenika V, Lutz AM, Beaulieu CF, Bucknor MD. Detection and prevalence of variant sciatic nerve anatomy in relation to the piriformis muscle on MRI. Skeletal Radiol 2017;46:751-7.

72. Sanchez-Gonzalez J, Luna A. DWI at 3T: Advantages, disadvantages, pitfalls, and advanced clinical applications. In: Luna A, Ribes R, Soto JA, editors. Diffusion MRI outside the brain: a case-based review and clinical applications. Springer Berlin Heidelberg, 2012:51-73.

73. Wada K, Goto T, Takasago T, Hamada D, Sairyo K. Piriformis muscle syndrome with assessment of sciatic

nerve using diffusion tensor imaging and tractography: a case report. Skeletal Radiol 2017. [Epub ahead of print].

74. Boyer RB, Kelm ND, Riley DC, Sexton KW, Pollins AC, Shack RB, Dortch RD, Nanney LB, Does MD, Thayer WP. 4.7-T diffusion tensor imaging of acute traumatic peripheral nerve injury. Neurosurg Focus 2015;39:E9.

75. Li R, Liu Z, Pan Y, Chen L, Zhang Z, Lu L. Peripheral nerve injuries treatment: a systematic review. Cell Biochem Biophys 2014;68:449-54.

76. Yamasaki T, Fujiwara H, Oda R, Mikami Y, Ikeda T, Nagae M, Shirai T, Morisaki S, Ikoma K, Masugi-Tokita M, Yamada K, Kawata M, Kubo T. In vivo evaluation of rabbit sciatic nerve regeneration with diffusion tensor imaging (DTI): correlations with histology and behavior. Magn Reson Imaging 2015;33:95-101.

77. Gallagher TA, Simon NG, Kliot M. Diffusion tensor imaging to visualize axons in the setting of nerve injury and recovery. Neurosurg Focus 2015;39:E10.

78. Socolovsky M, Malessy M, Lopez D, Guedes F, Flores L. Current concepts in plasticity and nerve transfers: relationship between surgical techniques and outcomes. Neurosurg Focus 2017;42:E13.

79. Simon NG, Kliot M. Diffusion weighted MRI and tractography for evaluating peripheral nerve degeneration and regeneration. Neural Regen Res 2014;9:2122-4.

80. Simon NG, Spinner RJ, Kline DG, Kliot M. Advances in the neurological and neurosurgical management of peripheral nerve trauma. J Neurol Neurosurg Psychiatry 2016;87:198-208.